Polymer Testing 140 (2024) 108627

Contents lists available at ScienceDirect

Polymer Testing

journal homepage: www.elsevier.com/locate/polytest

Innovative 3D-printed devices for water pollutant removal: Comprehensive review on printing parameters, composition, properties and performances of the latest 3D-systems

Roberto Scaffaro [a,b,*], Maria Chiara Mistretta [a,b], Marta Balsamo [a,b]

[a] Department of Engineering, University of Palermo, Viale delle Scienze, 90128, Palermo, Italy
[b] INSTM, Consortium for Materials Science and Technology, Via Giusti 9, 50125, Florence, Italy

ARTICLE INFO

Keywords:
3D printing
Additive manufacturing
Water pollution
Pollutants removal
Environmental remediation
Functional materials

ABSTRACT

Water pollution is one of the most pressing problems of our time; in fact, it contributes to 24 % of global deaths. Therefore, finding an effective and efficient solution is crucially important. In this regard, systems based on polymers and containing, often, fillers, intended for potential water pollutant removal are well established. Recently, simultaneously with the impressive spread of 3D printing, the production of these systems by various additive manufacturing processes is gaining popularity, enabling the rapid production of complex geometries, high porosity, large surface area and mechanical strength. These systems, to date, are becoming particularly competitive with 2D or 1D systems produced by other methods, so understanding them fully is essential. Therefore, here we provide a review of the most recent advances in the field of manufacturing 3D systems for water remediation. First, a brief introduction is proposed on the cathegory of 3D printing, making a distinction between Material Extrusion (MEX) and non-Material Extrusion (non-MEX) systems, and the main performance parameters of water pollutant removal. Next, the process parameters, composition, and morphological and chemical-physical properties of the latest 3D systems are discussed in detail. In the last part, an overview is given of the functional properties of these systems, in terms of removal efficiency and reusability, which is crucial in an ideal life cycle of such systems. In conclusion, the main outcomes and future perspectives for the production of more efficient systems are provided.

1. Introduction

Environmental pollution is one of the most urgent problems of our time, as it directly affects the quality of human life. According to the World Health Organization (WHO), 24 % of global deaths were linked to environmental pollution and climate change, especially in the South East Asia and Western Pacific regions. Between 2030 and 2050 an additional 250.000 deaths per year are expected, with an annual health cost estimated to be between USD 2–4 billion by 2030. Among the 24 % mortality risks attributable to global pollution, a predominant effect is observed on noncommunicable diseases, including cancer, cardiovascular and respiratory diseases, but also on infections and parasitic diseases mainly affecting the lower respiratory system [1]. Water pollution has a lower mortality risk than other forms of pollution, so it is an often underestimated threat, unlike other forms of pollution, such as air pollution, which, on the other hand, is among the most easily visible and studied types [2,3]. However, according to the UN World Water Development Report 2024, ensuring the treatment of polluted water is the main socio-economic driver for billions of people and, among the goals of the ONU 2030 Agenda for Sustainable Development, there is the clean-up and remediation of polluted water [4].

Besides changing the physical characteristics and aesthetic qualities of water, water pollution can often lead to its toxicity. It is, therefore, essential to understand the types of water pollutants, which may be released directly into the water or derived indirectly from other forms of pollution, for example through groundwater or rainwater polluted by soil and air respectively. Common pollutants include pesticides (herbicides and insecticides), dyes, oils, harmful chemicals (nitrite, ammonium nitrate), heavy metals, halogens, pharmaceuticals or drugs, radioactive pollutants and pathogens, all harmful substances that can accumulate in the tissues of living organisms, causing damage and disease [5–7]. For these reasons, attention is being focused on the

* Corresponding author. Department of Engineering, University of Palermo, Viale delle Scienze, 90128, Palermo, Italy.
E-mail addresses: roberto.scaffaro@unipa.it (R. Scaffaro), mariachiara.mistretta@unipa.it (M.C. Mistretta), marta.balsamo01@unipa.it (M. Balsamo).

https://doi.org/10.1016/j.polymertesting.2024.108627
Received 27 August 2024; Received in revised form 24 September 2024; Accepted 31 October 2024
Available online 1 November 2024

development of water remediation processes that are environmentally friendly, low-cost to implement, and highly efficient. In particular, the most widely used approaches include chemical treatments, adsorption, electrochemical oxidation and photodegradation of pollutants, or physical filtration processes and even biological treatments [8–10].

Over the last years, an increase in the application of polymeric materials as efficient systems for pollutants removal from water was observed. Typically, polymeric materials in various physical forms such as electrospun nanofibers, membranes, films or porous systems play a crucial role in decontamination processes [11]. Thus, while the use of traditional methods (electrospinning, phase inversion …) for the production of one- or two-dimensional systems probably appears as the most popular and discussed method [12], its limitations have consistently emerged in most reviews, slowing its scale-up for water remediation, in term of cost, time, mechanical stability and environmental impact [13,14]. More recently, alternative production techniques of additive manufacturing or 3D printing are gaining attention in the field of water remediation, due to simplicity, sustainability, versatility and processing cost/time reduction. According to the scientific literature, in fact, 3D printing for the production of three-dimensional supports is a very promising technique because it allows the rapid generation of materials with geometric complexity, high surface area, tunable porosity and surface roughness, and mechanical stability, useful features in water remediation processes [15]. In addition, there are also advantages inherent to the production method such as speed, cost-effectiveness and the typical absence of harmful solvents, which are peculiar to every type of 3D printing processes. Moreover, the properties of systems produced by 3D printing are particularly adjustable, simply by varying printing parameters [16–18].

By performing an overview of published papers using “3D printing” and “water pollution” as keywords, it is clear that the attention of the scientific community has progressively increased over the years. Based on these extracted data, a survey of papers published on Scopus in recent years was carried out; in particular, the analysis was conducted on VOSViewer software and the results are shown in Fig. 1.

The results reveal the automatic generation of various clusters, indicating interdisciplinarity and the possibility of evaluating the topic from different perspectives. Many nodes concern the types of pollutants previously discussed and the impact of pollution (health risk, global warming …). This is followed by nodes on production technologies (Fused Deposition Modeling, sintering, stereolithography) and methods for removing pollutants (photocatalysis, adsorption, oxidation …). Significant focus is given to life cycle, recycling, reuse, costs, and efficiency. There are also points on the porosity and surface properties of systems, as well as the fillers to be inserted into polymer matrices, such as metal nanoparticles, silica, titanium oxide, bacteria, graphene, and so on, which are useful for providing specific properties to materials, especially in the context of pollutant removal.

In this context, R. Selvakumar et al. [19] provide a brief overview of three-dimensional absorbent systems, comparing them with two-dimensional systems. They highlight how the former, compared to the latter, can have a larger surface area, a three-dimensional pore network, better stability, and the possibility of recovery. However, the analysis is not up to date. Duduku Saidulu et al. [20], produce an interesting review focusing on the advantages of 3D printing in wastewater treatment in terms of material composition, performance, challenges, and sustainable assessment. However, their analysis is limited up to 2021, so considering the exponential growth on these topics in recent times, it cannot be considered complete to date. Other works are similarly addressed [21,22]. Snigdha Roy Barman et al. [23] on the other hand, produced a more recent analysis of 3D systems used in water treatment, concluding that 3D printing is a major step towards obtaining sustainable manufacturing solutions in wastewater treatments. In parallel, Shabnam Siddiqui et al. [24] produced a review about the emerging trends in the development of 3D printed polymer composite systems for environmental application in various fields. Other works in

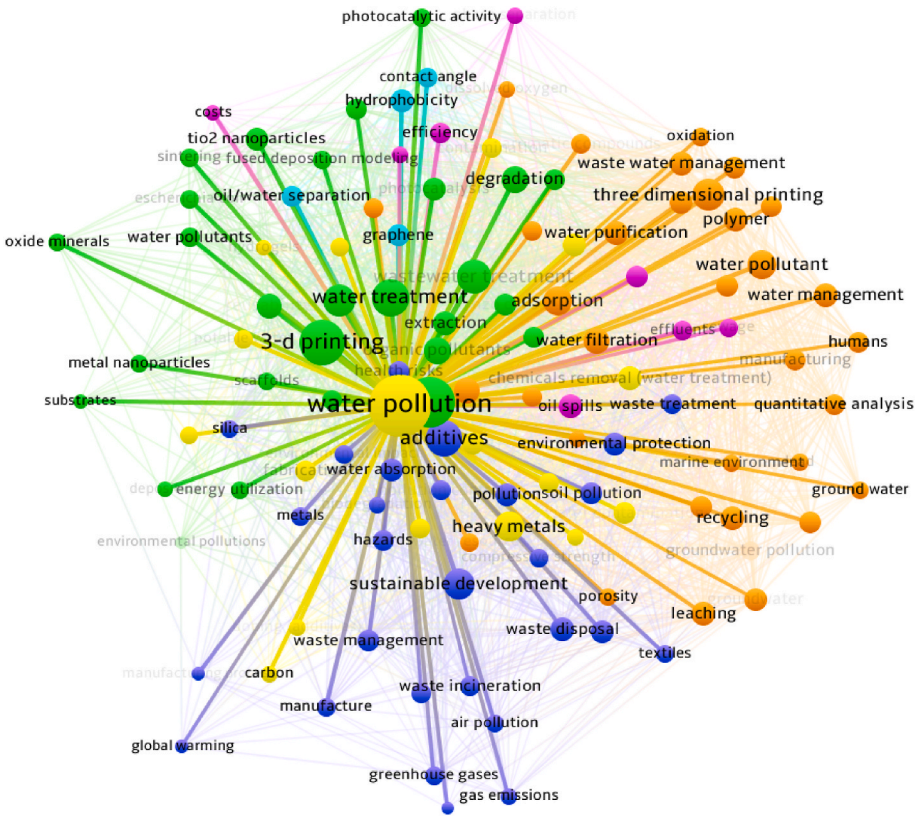

Fig. 1. VOSViewer map created by using papers present in Scopus database with “water pollution” and “3D printing” as keywords. Terms have been extracted by papers title and indexed keywords. Only terms with a minimum of 5 occurrences were taken into account.

this context, however, focus on specific printing techniques, such as Direct Ink Writing (DIW) [25], or on specific types of materials [26–28], as well as on specific types of water treatment [29,30].

Therefore, given the relevance of the topic in the field and the need to understand and learn about even the most recent and innovative proposals, it is of paramount importance to have an up-to-date perspective. This allows to obtain a comprehensive survey of the available possibilities, facilitating the selection of optimal combinations, considering the effectiveness and unique advantages of 3D printing in the context of environmental remediation. In this review, we provide an overview of the latest 3D polymer systems produced with 3D printing for water treatment. In particular, after describing the main mechanisms and parameters of water remediation performances, we provide an overview distinction between the different production techniques of 3D printing. Subsequently, we present materials, process parameters, shape and main morphological and chemical-physical characteristics of the systems produced, making a distinction between systems based on extrusion processes (Material Extrusion) and on other printing processes (non-Material Extrusion), which will have different production parameters and properties. Furthermore, the analysis shifts to the functional properties of the devices, i.e. their performance in the absorption of pollutants, with a focus on the type of pollutant and its removal technology, making a distinction between removal by degradation and isolation of the pollutant. Finally, emphasis is given to the possibility of reusing the system for multiple cycles. In conclusion, challenges and future perspectives on polymer systems produced by 3D printing for water remedition are described.

2. Key parameters of water remediation performance

Before exploring the production techniques, composition, and properties of 3D systems for pollutant removal from water, it is useful to provide a brief overview of the key parameters of water remediation performance. Understanding these parameters will allow us to comprehend how the system's characteristics can be adjusted to maximize performances.

After the treatment, the efficiency of pollutant removal is evaluated by the Removal Efficiency (R_E), which is one of the key parameters to assess the performance of remediation. R_E can be evaluated using Equation (1):

$$R_E = \frac{C_0 - C_f}{C_0} \text{ x } 100\% \quad (1)$$

where C_0 is the initial concentration of pollutant in the solution, and C_f is the concentration measured after the treatment time (t_T), which can range from a few hours to several days and defines the treatment's efficiency itself. The pollutant removal efficiency is directly influenced by the interaction between the pollutant and the 3D system, thus it is heavily dependent on the characteristics of the latter, primarily its surface properties such as wettability, porosity and the surface area, as they will determine the extent of contact with the pollutant. Therefore, in general, it has been demonstrated that 3D structures can have high surface areas and shapes that influence the fluid dynamics of the polluted solution, varying the contact time between biomass and pollutant, thus enhancing removal efficiency [31,32].

In some cases, after the first treatment, the support can be reused under the same conditions to assess its reusability across multiple cycles, determining the variation of R_E for each cycle. The reusability cycles are a highly significant efficiency parameters, as reusing the support would reduce the environmental impact of its production and disposal. The possibility of reusing the support depends on the characteristics of the material, namely its long-term mechanical/physical stability. Indeed, a biodegradable material may be used for fewer cycles compared to a biostable polymer, or for shorter treatment times. Moreover, a 3D support is likely to have superior mechanical performance compared to 1D or 2D one; therefore, it will be tested for longer reuse cycles [33]. The reusability will also depend on the possible filler immobilized in the polymeric matrix, namely the stability and the condition of immobilization on the support. Therefore, the ideal life cycle of such a system should include the production of the system, its use for pollutant removal, and its regeneration for subsequent efficient reuse (RE ≈ 100 %).

In the following paragraphs, it will be discussed in detail how by selecting compositon, production techniques and parameters, it is possible to regulate the performance of remediation processes and their environmental impact. Therefore, it is essential to clarify which are the main 3D printing technologies used in this context.

3. Generality on 3D printing processes

3D printing, or additive manufacturing, allows the creation of three-dimensional objects layer by layer from computer-aided design (CAD) file and enables the production of prototypes according to specific customer or project requirements. Recently, this processing approach is developing considerably in various contexts, due to its versatility, rapidity and increasingly affordable costs [34,35]. Products made by 3D printing processes can have intricate geometries with a high surface area, can be porous or dense and mechanically resistant. These aspects appear to be very useful in various application contexts, certainly including environmental remediation, as they allow for high active area for the removal of pollutants and the mechanical stability facilitates the reuse of the structure [36,37].

Following the ISO/ASTM 52900 standard on additive manufacturing terminology, it is possible to classify the main 3D printing techniques into two categories, as shown in Fig. 2: those based on an extrusion process and those that are not. The former will be classified in the following as Material Extrusion (MEX) 3D Printing, a process in which material is selectively dispensed through a nozzle or orifice. Consequently, the others will be included in the term non-Material Extrusion (non-MEX) 3D Printing.

Within the two categories, further distinctions can be made between fused and non-fused technologies. In particular, for MEX 3D Printing, the fused or melt MEX technology is an additive manufacturing technology where a polymer is heated to a specific temperature (T nozzle) in a chamber, so that it melts, and then extruded from the nozzle in filament form, to create objects layer by layer [38]. These processes are fast, cheap and solvent-free, but they generally involve high temperatures.

As an alternative to melt technologies, ink MEX 3D printing allows working at much lower temperatures, as the material to be extruded can be typically an hydrogel with sufficient viscosity to guarantee layer-by-layer deposition through an appropriately sized nozzle: the solidification and stabilization of the artefact is generally achieved through a physical, chemical, ionic or light cross-linking process [39]. In this case, the provided printing conditions are suitable for the incorporation of cells or other biomass (bacteria, enzymes …) inside the ink prior to print (bio-ink), useful in biomedical applications, but also in bioremediation [40]. This latest type of hydrogel MEX printing is called 3D Bioprinting (3DBP). In addition, the Direct Ink Writing (DIW) is a layer-by-layer MEX printing technique involving the pressure deposition of a visco-elastic ink, polymeric or not, through a nozzle and subsequent stabilization of the structure [41].

Non-MEX 3D Printing technologies, on the other hand, are typically passive technologies with local consolidation of the device. In this category, it is also possible to make a distinction between fused and non-fused technologies. Fused technology is called Powder Bed Fusion, according to the standard; it is a process in which thermal energy selectively melts regions of a powder, also known as Selective Laser Sintering (SLS) [42].

Non-melt processes are included in the Vat Polymerization category, defined by the standard as a process in which liquid photopolymer in a vat is selectively cured by light-activated polymerization. These

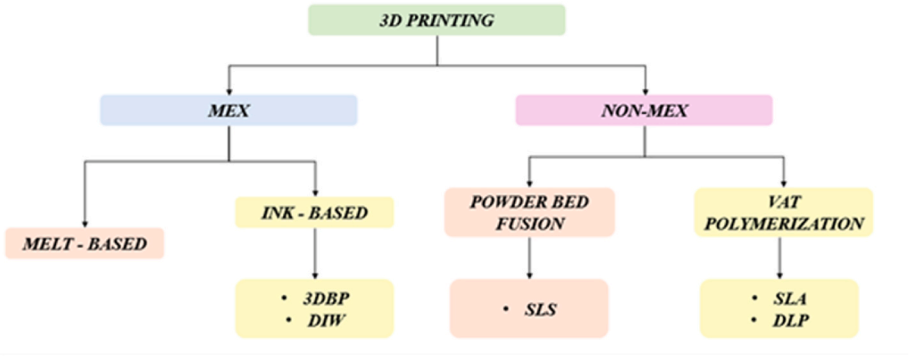

Fig. 2. Overview on 3D printing processes.

processes include stereolithography (SLA) and Digital Light Processing (DLP), where the substantial difference is in the curing method: instead of a mirror, a digital light projector is employed in the latter to refletct a laser source [43,44].

Each of these technologies is suitable for the production of three-dimensional polymer-based systems to be used in the field of water remediation for the absorption of pollutants, with appropriate differences in terms of composition, printing parameters and thus system properties.

4. Polymeric materials, printing parameters and main properties of water remediation 3D printed systems

Polymeric materials are currently widely used for the production of three-dimensional systems using the 3D printing techniques discussed above [45–47]. This is due to the fact that they are well suited to such production processes and, in addition, are generally cheaper, easier to work with and more versatile than other materials. These polymeric materials may be biostable or biodegradable depending on the duration of the application, they must guarantee adequate chemical-physical properties and, in this context, they have to remove efficiently pollutants, properties that may be adapted by the addition of additives or fillers. The choice of materials and fillers is closely related to the choice of the 3D printing technology. The complex architectures and mechanical stability of the systems are important peculiarities allowed by these techniques. Exploiting the previous distinction between extrusion-based and non-extrusion-based production technologies, in the following, the types of polymers, fillers, printing conditions and properties of the resulting 3D systems for water remediation will be analyzed in detail.

4.1. Material Extrusion (MEX) systems

4.1.1. Melt MEX systems

The category of MEX systems is based on melt technology.In this context, the most commonly used polymeric material is polylactic acid (PLA), but other thermoplastic polymers are also used, such as acrylonitrile butadiene styrene (ABS), polyamides (PA), polycaprolactone (PCL), polypropylene (PP), polyethylene (PE), polyurethane (PU), polyvinyl alcohol (PVA), polystyrene (PS), glycol-modified polyethylene terephthalate (PETG) [48–51].

Composition, printing parameters and main characteristics of polymer-based systems for water remediation recently produced by 3D melt MEX printing) are listed thoroughly in Table 1.

4.1.1.1. Polylactic acid-based. Polylactic acid (PLA) is one of the most popular materials for melt MEX 3D printing due to its distinctive properties and characteristics. It is often used together with fillers to improve its characteristics and to produce superior printed parts, by changing its printing parameters [83,84]. In the context of pollutant removal, fillers provide specific properties to the polymer, such as absorption capacity or degradation of specific contaminants.

For example, the use of metal oxides as fillers in polymeric matrix is an effective strategy to improve the properties of composite materials and to enhance their ability to remove pollutants, generally through catalytic processes [85]. Among these, titanium oxide (TiO2) is a photocatalytic substance that has been widely studied for its capability to breakdown pollutants [86,87].

For example, Pablo Ortega-Columbrans et al. [52] produced a cylindrical gyroidal scaffold with a diameter of 2.5 cm based on PLA. Specifically, they have produced a filament PLA:TiO_2 85:15 vol%, which was printed by a printer with a 0.4 mm diameter nozzle at 160 °C and a printing speed of 20 mm/s. The gyroidal pattern ensured high surface area structure, with macropores diameters d_p = 400–900 μm. Andrew D. McQueen et al. [53] produced PLA:TiO_2 80:20 wt% filaments and subsequently printed it at a nozzle temperature (0.4 mm) of 210 °C. They produced a disk structure with a diameter of 8.5 cm and 50 % infill, which provided macropores and a light exposed surface area of 56.75 cm^2. Sangiorgi et al. [54] produced a similar structure in PLA with 30 % wt of TiO_2. The disk system was printed at 185 °C and 40 mm/s and 30 % infill. Kennedy et al. [55] realized a geometrically complex structure by printing PLA:TiO_2 filaments with high TiO_2 content (34 % w/w). The nozzle temperature of 215 °C was slightly higher than the previous seen above, probably due to the higher filler content. The device had a diamond latex tetrahedron shape and is a few cm^3 in size; the printing speed was 45 mm/s and the infill was 20 %, allowing for a macroporous structure with a surface area of 7521 mm^2.

Photocatalytic activity is also provided by other metal oxides species, such as zinc oxide (ZnO) [88]. For example, Kun Li et al. [56] produced a square PLA-based substrate, which was subsequently covered with ZnO cold plasma discharge (CPD), with a maximum grafting rate equal to 8 %. The fractal surface of the system ensures a high surface area. The same authors also produced another similar system, namely a PLA-based fractal square [57]. This is printed from a nozzle (0.4 mm) at 210 °C with a printing speed of 20 mm/s. The 20 % infill and fractal surface ensured high surface area. Again, the system was subsequently coated via CPD with ZnO coupled with bismuth molybdate (Bi_2MoO_6), coupling that ensures enhanced photocatalytic performance. The system had a water contact angle (WCA) > 90°, so it is hydrophobic: this could concentrate organic pollutants on the surface and thus improve treatment efficiency.

Another metal oxide widely used for the removal of pollutants is magnetite (Fe3O4), due to its high surface area and chemical reactivity [89]. Kihoon Kim et al. [58] printed (0.4 mm nozzle) a cylindrical PLA system on which Fe(III) oxide was subsequently immobilized, enhancing the absorbent properties and hydrophilicity. The cylinder had macropores diameter d_p = 0.8 mm and high surface area (>6 × 10^4 mm^2). S. Fernandez-Velayos et al. [59] produced cylindrical systems by printing PLA:Fe_3O_4 85:15 % wt pellets at 185 °C (nozzle 0.4 mm). The system provided an internal grid with macropores of diameter d_p = 5 mm, which guaranteed a high surface area and interesting velocity profiles inside a fixed-bed reactor, as shown in Fig. 3: in fact, this shape ensured

Table 1
Composition, printing parameters and main characteristics of polymer-based systems for water remediation produced by 3D melt MEX printing recently.

Ref	Composition	Filler	Filler Conc	Filler Imm.	Nozzle Diam.	T Nozzle	Printing Speed	Infill	Shape	Porosity	SA	WCA	Mechanical Properties
[52]	PLA	TiO2	15 %	PRE	0.4 mm	160 °C	20 mm/s	/	Gyroidal scaffold	d_P = 400–900 μm	/	/	/
[53]	PLA	TiO2	20 %	PRE	0.4 mm	210 °C	/	50 %	Disk	Macropores	56.75 cm^2	/	/
[54]	PLA	TiO2	30 %	PRE	0.3–0.5 mm	185 °C	40 mm/s	30 %	Disk	Macropores	/	/	/
[55]	PLA	TiO2	34 %	PRE	/	215 °C	45 mm/s	20 %	Diamond lattice tetrahedron	Macropores	7521 mm^2	/	/
[56]	PLA	ZnO	8 %	POST	/	/	/	/	Square	/	/	/	/
[57]	PLA	ZnO/ Bi2MoO6	/	POST	0.4 mm	210 °C	20 mm/s	20 %	Square	/	/	>90°	/
[58]	PLA	Fe(III)	/	POST	0.4 mm	/	/	/	Cylinder	d_P = 0.8 mm	>6 × 10^4 mm^2	<90°	/
[59]	PLA	Fe3O4	15 %	PRE	/	/	/	/	/	/	/	/	/
[56]	PLA	MOF	2.5 %	POST	/	/	/	/	Square	/	/	/	/
[60]	PLA@TCNFs	MOF	/	POST	0.4 mm	215 °C	45 mm/s	10 %	Cuboid	Macropores	/	/	E = 1200 MPa
[61]	PLA	GO/ Chitosan	9 %	POST	23G	230 °C	350 mm/ s	/	Fish Mouth	Hierarchically porous; P = 97 %	/	<90°	CS = 74.5 MPa
[62]	PLA	GO	/	POST	0.4 mm	200 °C	40 mm/s	40 %	Cylinder	Macropores	/	/	/
[63]	PLA	Carbon Black	21.8 %	PRE	0.4 mm	215 °C	/	50 %	Cylinder	A_P = 0.2 mm^2	/	/	/
[64]	PLA	Carbon Nitride	/	POST	/	/	/	/	Cylinder	Dense	/	/	/
[65]	PLA	MA	2 × 10^6 cells/ ml	POST	6 μm	220 °C	100 mm/ s	/	Cylinder	Porous	/	/	CS = 110 kN/ m^2
[66]	PLA	Laccase		POST	/	185 °C	/	/	Cylinder	Macropores	5.42 cm^2	/	MS = 10.7 MPa
[67]	PLA/PBAT	MA	30 %	PRE	0.4 mm	180 °C	50 mm/s	/	Grid	Hierarchically porous	/	/	TS = 20 MPa
[68]	PLA	Zeolite	16 %	PRE	0.4 mm	195 °C	30 mm/s	/	Cross	Micropores	/	/	/
[69]	PLA	Zeolite	32 %	PRE	0.4 mm	210 °C	30 mm/s	20 %	Flower	Macropores	/	/	/
[70]	PLA	HAP	15 %	PRE	0.4 mm	230 °C	30 mm/s	/	Disk	Macropores; P = 40 %	/	/	/
[71]	PLA/PBS/ PVA	CSP	30 phr	PRE	0.4 mm	180 °C	60 mm/s	/	Scaffold	P = 48.37 % d_p = 6 μm	0.67 m^2/g	/	/
[72]	PLA	TCNF, ChNF	/	PRE	0.4 mm	220 °C	55 mm/s	10 %	Hourglass	d_P = 1.5 mm	/	/	E = 1000 MPa, E = 900 MPa
[73]	PS	TiO2	20 %	PRE	/	240 °C	50 mm/s	/	Rectangulare	Dense	200 mm^2	/	/
[74]	LDPE	TiO2	1 %	PRE	0.4 mm	200 °C	1000 mm/min	/	Square mesh	Macropores	/	/	/
[75]	PETG	TiO2, CNT	3 %, 0.5 %	PRE	/	235 °C	/	60 %	Helical	/	/	/	/
[76]	PETG/PVA	/	/	/	0.4 mm	230 °C	45–50 mm/s	/	Cartridge	Micropores	/	>90°	/
[77]	ABS	ZnO	10 %	PRE	/	220 °C	/	100 %	Network of cubes	Macropores	/	/	/
[78]	ABS/TPU	$CaSiO_3$	40phr	PRE	0.4 mm	200 °C	50 mm/s	/	Scaffold	Macropores	0.864 m^2/g	/	/
[79]	ABS	POM	/	POST	/	240 °C	/	/	Square mesh	Highly porous	/	<90°	/
[80]	PA	Carbon Fiber	15 %	PRE	/	270 °C	30 mm/s	/	Disk	Macropores	2859.5 mm^2	/	/
[81]	PCL/SA	/	/	/	/	135 °C	12.3 mm/s	/	Tube	Dense	/	/	/
[82]	MB	SLP, NPK	10 %	PRE	0.4 mm	160 °C	50 mm/s	100 %	Rectangular	Micropores	/	/	E = 707 MPa

low velocity of the polluted fluid in the region and, therefore, longer contact times with the 3D system, which has improved treatment efficiency.

Polymeric systems are also found together with Metal-Organic Frameworks (MOFs), a class of materials with tunable porous structure, crystallinity and high surface area [90,91], frequently used for the removal of pollutants, sometimes with PLA. For example, Kun Li et al. [56] coated the same fractal squares in PLA seen before in the same work with MOFs, demonstrating versatility of the process. Natalia Fijoł et al. [60] produced PLA-based composite filaments reinforced with TEMPO (2,2,6,6-tetramethylpiperidine-1-oxyl radical)-mediated oxidized cellulose nanofibres (TCNF). The cuboid systems (rectangular parallelepiped

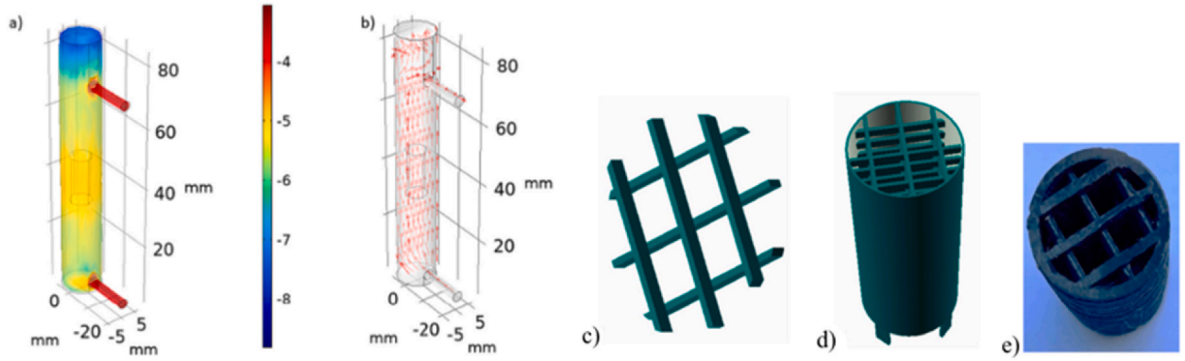

Fig. 3. (a) Velocity profiles computed on the reactor equipped with PLA@Fe_3O_4 3D systems under steady state conditions; (b) Arrow plot representing the velocity vectors of the fluid along the reactor; (c) internal mesh of 3D system, (d) entire 3D system with internal mesh, (e) printed system. Reprinted with permission [59]. Copyright 2024, Elsevier.

of few cm^3) were printed with a nozzle (0.4 mm) at 215 °C and a printing speed of 45 mm/s and then MOFs were anchored on the surface. The systems were few cm^3 in size and macroporous due to the 10 % infill. Despite the porosity, they maintained good mechanical properties, with Young's modulus equal to 1200 MPa.

Moreover, the absorption of pollutants is often enhanced by the addition of carbon nanofillers of various kinds. In fact, these materials offer high specific surface areas and numerous active sites, making them ideal for adsorption of contaminants [92,93]. We refer to carbon nanotubes (CNTs) and graphene oxide (GO), for example. In this contest, G. Zhou et al. [61] produced a pyramid system by printing PLA from a nozzle (23G) at 230 °C and printing speed of 350 mm/min. The system had an interesting shape of a biomimetic fish mouth, to demonstrate processing versatility, and appeared hierarchically porous, with a porosity (P) of 97 %. The system was subsequently coated using a suspension of GO and chitosan (GO content equal to 9 % wt), both fillers with good adsorptive properties, which gave the system hydrophilicity (WCA <90°) and higher compressive strength (CS = 74.5 MPa). Sung-Sil Park et al. [62] produced a cylindrical PLA system by printing a filament from a nozzle (0.4 mm) at 200 °C with a printing speed of 40 mm/s, on which GO was subsequently immobilized. The system had an internal grid, which was guaranteed by a 40 % infill, generating macroporosity and high surface area.

In addition, carbon black and carbon nitride are also often used for the removal of pollutants in PLA systems [94]. Luke A. Lagalante et al. [63], for example, produced a cylindrical system by printing a PLA filament containing 21.83 % carbon black at 215 °C (nozzle diameter equal to 0.4 mm). The 50 % infill generated macroporosity, with pore area $A_P = 0.2\ mm^2$. Instead, Manuel Penas-Garzon et al. [64] produced a dense cylindrical PLA system, on which a carbon nitride powder is subsequently immobilized, generating a porous texture on the device.

Polymers are also used in combination with biomasses such as bacteria, enzymes or microalgae (MA); in these systems, the metabolic and catalytic abilities of these organisms are exploited to degrade or adsorb contaminants, in bioremediation processes [95,96]. In this regard, Patricia Laura Marconi et al. [65] generated a hollow cylindrical system by printing a PLA filament from a 6 μm nozzle at 220 °C and printing speed of 100 mm/s. Within the few cm^3 system, MA (2×10^6 cells/ml) were successively immobilized. The produced system was porous and mechanically resistant (CS = 110 kN/m^2), to ensure the survival of the cells. Instead, Agnieszka Rybarczyk et al. [66] immobilized the laccase enzyme on a cylindrical system printed with a PLA filament at 185 °C. In detail, the immobilization occurred post production of the device, which has a particular geometric conformation that has guaranteed macroporosity and high surface area $S_A = 5.42\ cm^2$. Furthermore, the system was mechanically resistant with a maximum strength MS = 10.7 MPa. Alternatively, but less commonly in melt technologies given the high temperatures, biomass can be immobilized in the filament before it is used to print the device. Xinshu Xia et al. [67], for example, printed a PLA/PBAT-based filament containing 30 % MA. The filament was printed from a nozzle (0.4 mm) at 180 °C and printing speed of 50 mm/s, to create a grid with hierarchical porosity and good mechanical properties (tensile strength TS = 20 MPa).

Another category of fillers used in combination with polymeric systems for the absorption of pollutants are zeolites, because of their high surface area and high adsorption sites [97,98]. In this regard, Alan J. Kennedy et al. [68] printed a cross-shaped microporous device, starting from a PLA filament containing 16 % wt of zeolite. The filament was printed from a 0.4 mm nozzle at 195 °C with printing speed 30 mm/s. The same authors subsequently printed PLA filaments containing 32 % wt zeolite, using higher nozzle temperatures (210 °C) [69]. The produced system had a flower-like geometry and the 20 % infill makes it macroporous.

Alternatively, hydroxyapatite (HAP) has also recently been used in the field of environmental remediation, due to its adsorption capabilities and porous structure [99]. For example, Natalia Fijol et al. [70] printed a PLA filament containing HAP, at 230 °C and printing speed of 30 mm/s, from a 0.4 mm nozzle. The structure produced was a grid disk with macropores generated during the printing phase, with an overall porosity P = 40 %.

Finally, PLA is often printed together with natural fillers, which exhibit excellent absorbent properties [100]. For example, Yinglian Zheng et al. [71] printed polylactic acid/polybutylene succinate/polyvinyl alcohol (PLA/PBS/PVA) filaments containing 30 phr of camellia seed powder (CSP), where PVA was employes as a porogen and CSP provided adsorption sites. The filaments were printed at 180 °C (nozzle 0.4 mm) and printing speed 60 mm/s. Scaffolds with P = 48.37 %, pore size $d_p = 6$ μm and high surface area $S_A = 0.67\ m^2/g$ were fabricated. In another work by Natalia Fijoł et al. [72], they produced an interesting hourglass architecture with large surface area by printing PLA filaments containing polysaccharide nanofibers (TEMPO-oxidized cellulose nanofibers (TCNF) or chitin nanofibers (ChNF)), as shown in Fig. 4, where these natural fillers acted as reinforcement and active sites for adsorption.

The filaments were printed from nozzles (0.4 mm) at 220 °C, printing speed 55 mm/s and infill 10 %. The porous structure had macropores, arranged according to various levels of porosity, with diameters d_p = 1.5 mm. Both fillers made the systems mechanically resistant, with compressive elastic modulus E about to 1000 MPa and 900 MPa, respectively.

4.1.1.2. Other polymeric systems. As already anticipated, PLA is not the only polymeric material used in melt MEX 3D printing processes.

For example, Z. Viskadourakis et al. [73] used polystyrene (PS) mixed with TiO_2 (20 % w/w) to produce filaments to be printed at 240 °C and a printing speed of 50 mm/s. The devices produced were

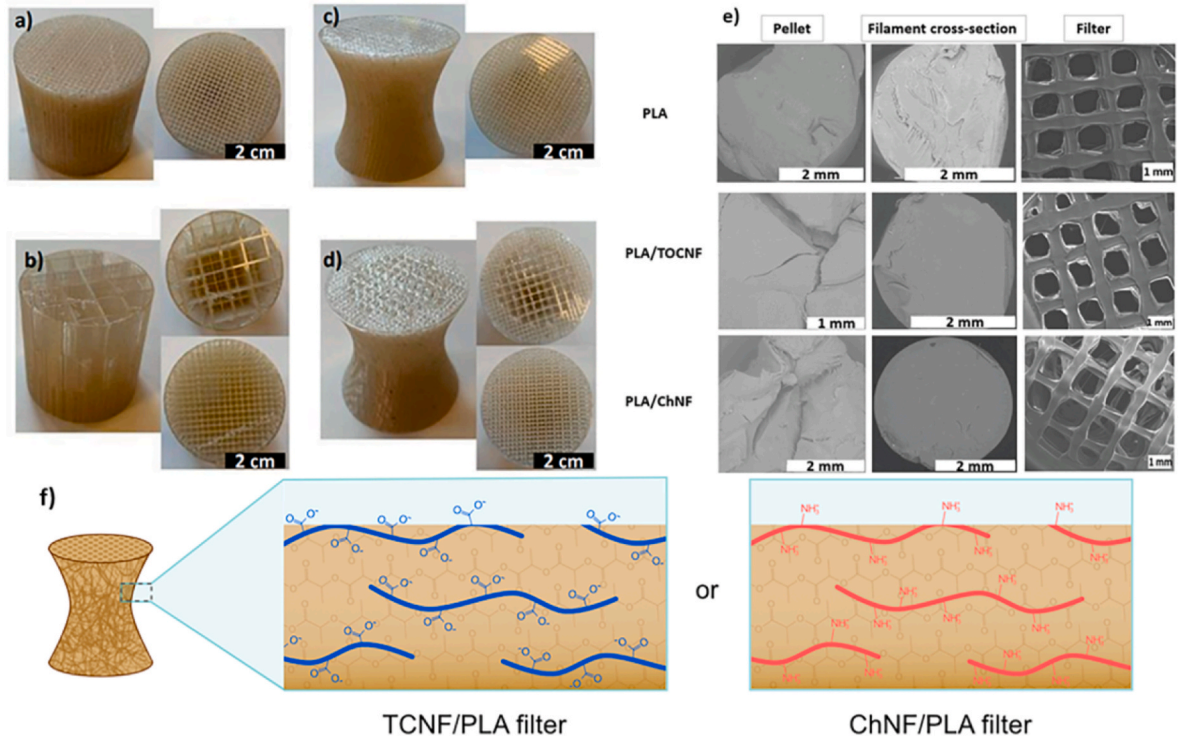

Fig. 4. 3D printed system (a) uniform porosity cylinder, (b) three level gradient porosity cylinder, (c) hourglass-shaped uniform porosity system, (d) hourglass shapes two level gradient porosity system, (e) SEM images of pellet, filament and 3D systems section for PLA and both the composite; (f) graphic representation of dispersion of fibers. Reproduced with permission [72]. Copyright 2023, Elsevier.

dense and rectangular in shape and had cylindrical pillars on the surface, allowing the surface area to be increased to 200 mm^2.

Instead, María J. Martín de Vidales et al. [74] used 1 % w/w TiO_2 together with low density polyethylene (LDPE) to generate square mesh using filaments printed at 200 °C (nozzle 0.4 mm) and printing speed 1000 mm/min. The devices presented macroporosity provided by the mesh, to obtain a high surface area. Kristina Miklec et al. [75] mixed TiO_2 and carbon nanotubes (CNT) (3 % and 0.5 % respectively) with glycol-modified polyethylene terephthalate (PETG) and subsequently printed helical structures from filaments at 235 °C with an infill density of 60 %.

Ankur Jyoti Thakuria et al. [76] recently used PETG/PVA filaments to produce hydrophobic (WCA>90°) discoidal cartridges of 20 mm diameter, where the PVA acted as a porogen to generate microporosity. The filaments ware printed at 230 °C and printing speed of 45–50 mm/s.

Another material used in 3D printing is acrylonitrile butadiene styrene (ABS). For example, Sidra Waheed et al. [77] produced ABS filaments with 10 % wt of ZnO, to be printed at 220 °C and 100 % infill to produce a network of interconnected cubes of a few cm^3, with CAD generated macroporosity. In detail, the filler in the printed device was chemically converted to zeolitic imidazolate framework (ZIF), a category of MOFs with absorbent capacities. Similarly, Zhen Liu et al. [78] printed ABS/TPU-based filaments containing 40 phr of microporous calcium silicate (CaSiO3) at 200 °C and 50 mm/s. The macroporous scaffold with spiral skeleton and high surface area (0.864 m^2/g) was chemically treated to convert the filler into Ca-MOF, with adsorbent capabilities. ABS was also printed by Yuanchun Ji et al. [79] at 240 °C to produce an hydrophilic highly porous square mesh. The structure was then functionalized with polyoxometalate anions (POM), as heavy metal binding sites.

A further material which can be employed in melt MEX, but which is known to require high printing temperatures, is polyamide (PA) [51]. In this context, Camila Scheid et al. [80] printed PA filaments containing 15 % carbon fibres at 270 °C and 30 mm/s. The structure produced is honeycomb-like disk, with macroporosity and surface area $S_A = 2859.5$ mm^2.

Lower printing temperatures are expected for polycaprolactone (PCL) [101]. In fact, Ioannis L. Liakos et al. [81] produced filaments based on PCL and 30 % sodium alginate (SA), where the latter is well known to have heavy metal adsorption capacities [102]. The filaments were printed at 135 °C and 12.3 mm/s to produce dense tubular structures.

Another material that can be printed at low temperatures is Mater Bi (MB), a commercial blend of biodegradable co-polyesters, which has recently emerged as an option for green composites for melt MEX [103, 104]. Scaffaro et al. [82] produced filaments based on MB, using Solanum Lycopersicum (tomato plant, SLP) 10 % wt as filler, in which the natural filler has a high affinity for metal ions. The filaments were printed at 160 °C (nozzle 0.4 mm) and 50 mm/s to produce rectangular specimens with printing process-induced porosity and good mechanical properties (E = 707 MPa). In addition to SLP, NPK fertilizer was also added to the filament for its controlled release, as it is soluble in water: the migration of NPK into water generated additional porosity in the device and increased the surface area.

4.1.2. Ink MEX systems

The category of MEX systems based on ink or bioink, involves the use of 3D Bioprinting (3DB) or Direct Ink Writing (DIW). In this context, the most commonly used polymeric materials are natural polymers such as alginate (Alg), chitosan, cellulose, hyaluronic acid (HA), gelatin, but also synthetic polymers, such as polyethylene glycol (PEG), Pluronic F127, polyvinyl alcohol (PVA), poly (ethylene glycol) dia-crylate (PEGDA) [39] and so on. Recently, geopolymers are also being used in 3D ink MEX-based printing processes to make systems used in water pollutant absorption applications, due to their porous structure, chemical stability and versatility of composition [105–108]. Composition, printing parameters and main characteristics of polymer-based systems for water remediation recently produced by 3D ink MEX printing are

listed in Table 2.

Alginate is a widely used material in ink MEX systems for water remediation, typically together with other polymers to improve their mechanical performance, printability or absorption properties. In addition, alginate biocompatibility makes it suitable for 3D Bioprinting (3DBP) processes, often mixed with other polymers to improve its rheological and mechanical properties. The possibility of using alginate-based ink in 3DBP for water remediation results in the incorporation of biomass for bioremediation processes. Unlike melt MEX systems of the same function [65,66], in these cases the use of low temperatures allows biomass to be immobilized PRE printing, often enabling an increase in immobilization efficiency.

For example, Seon-Won Yoon et al. [109], created a cylindrical system of a few mm^3 based on alginate (Alg)/methylcellulose (MC), immobilizing microalga (MA) Chlorella Vulgaris in the ink. The system presented macropores made by the printing process carried out at room temperature and printing speed of 10 mm/s, and then ionically cross-linked in $CaCl_2$. Jessica Condi Mainardi et al. [110] produced an ink based on alginate and chitosan, whose mechanical performance is enhanced by alumina. Bioremediation capabilities are enabled by the presence of bacteria (B) in the ink (32.5×10^8 cfu/mL). The ink was then printed at low temperatures by a 940 μm tip nozzle at 10 mm/s. The infill density of 67 % allowed for a high surface area and macropores of the lattice cubes system, which was chemically cross-linked using genipin as cross-linking agent. Instead, Yuan Li et al. [111] produced a lattice system based on thiolated sodium alginate and hyperbranched PEGDA containing yeasts. Specifically, the latter was encapsulated in ink preliminarily by generating yeast-laden hydrogel microparticles (HMPs) by droplet-based microfluidic preparation process, in order to enhance cell survival by compartmentalizing them in a granular hydrogel. Then a lattice of biocatalytic living materials was printed through a conical precision nozzle (610 μm) and 130 mm/min. The granular hydrogels were ionically cross-linked by using $CaCl_2$. A system with similar composition is realized at the same time by Yan Li et al. [112]. Specifically, they produced a bioink based on PEGDA/Alg/PVA and nanoclay (n-clay), in which PVA increased porosity and the nanofiller improved mechanical and absorption performance, as already observed in other works [122], containing bacteria (B) (1.2×103 CFU/g) with the capabilities of pollutant removal. The bioink was printed at room temperature from a flat tip needle (0.4 mm) at 200 mm/s to produce a grid with hierarchical porosity. The system was subjected to dual cross-linking: after extrusion, printed systems were

Table 2
Composition, printing parameters and main characteristics of polymer-based systems for water remediation produced by 3D ink MEX printing recently.

Ref	Composition	Filler	Filler Conc	Filler Imm.	Nozzle Diam.	Printing Speed	Infill	Cross-linking	Shape	Porosity	SA	WCA	Mechanical Properties
[109]	Alg/MC	MA	2×10^7 cells/ml	PRE	0.4 mm	10 mm/s	/	Ionic	Cylinder	Macropores	/	<90°	/
[110]	Chitosan/Alg @Allumina	B	32×10^8 cfu/ml	PRE	0.94 mm	10 mm/s	67 %	Chemical	Lattice	Macropores	/	/	/
[111]	PEGDA/Alg	Yeast	/	PRE	0.61 μm	130 mm/min	/	Ionic	Lattice	Hierarchical porosity	/	/	/
[112]	PEGDA/Alg/PVA@n-clay	B	1.2×10^3 cfu/ml	PRE	0.4 mm	200 mm/s		Dual	Grid	Hierarchical porosity	10 m^2/g		TS = 185 kPa, CS = 365 kPa
[113]	Alg/AM@HAP	Laccase	/	PRE	/	/	/	Dual	Grid	Macropores	/	/	/
[114]	Alg/F127-DA	MA/B	3.9-4x10^6 cells/g	PRE	0.4 mm	360 mm/min	/	Dual	Fiber	Micropores	/	/	/
[115]	F127-DMA/Alg	Laccase	4 mg/l	PRE	25G	6 mm/s	18 %	Light	Flower	Hierarchical porosity	2739 m^2	/	/
[116]	HA	B	50 μl/ml	PRE	/	/	/	Light	Grid	Macropores	/	/	/
[117]	F127-BUM	Yeast	10^6 cells/g	PRE	/	10 mm/s	45 %	Light	Grid	Macropores	/	/	/
[118]	Alg/Gelatin/PEI	/	/	/	/	/	/	/	Tablet	Micropores	9.907 m^2/g	<90°	/
[119]	PVA/AA	/	/	/	10 mm	15 mm/s	/	Light	Cylinder	Hierchical porosity	/	<90°	E = 4–5 MPa
[120]	Chitosan/DA Pluronic F-127	/	/	/	0.9 mm	5 mm/s	/	Light	Sheet	d_p = 4 mm	/	/	/
[121]	CNC/LAE	/	/	/	0.34 mm	10 mm/s	1.25 mm gap	/	Grid	Highly porous			
[122]	Alg/AA	n-clay	0.25 %	PRE	1 mm	15 mm/s	/	Electron Beam	Cube	/	/	<90°	E = 18 MPa
[123]	CNF/Alg	COFs	/	PRE	0.4 mm	/	/	Ionic	Grid	Hierarchical porosity	30 m^2/g	/	/
[124]	Alg/Gelatin	MOFs	13 %	PRE	0.21 mm	33 mm/s	/	Ionic	Grid	Hierarchical porosity	83 m^2/g	/	TS = 0.4 MPa, CS = 1.8 MPa
[125]	Cellulose	MOFs	67.5 %	PRE	0.4 mm	10–80 mm/s	/	/	Grid	Hierachical porosity	38 m^2/g	/	/
[126]	Cellulose	Fe_3O_4	26 %	PRE	0.84 mm	5 mm/s	/	Chemical	Lattice	V_p = 0.03 cm^3/g	30 m^2/g	/	/
[127]	PDA/BSA	GO		PRE	0.6 mm	20 mm/s	/	/	Cylinder	P = 90 %, d_p = 10 μm	9.86 m^2/g	>90°	/
[128]	PEI/PEG	GO + SiO_2	GO: 4.8 %	PRE + POST	/	/	780 μm gap	AVT	Scaffold	P = 94 %	>190 m^2/g	<90°	CS = 0.1–0.4 MPa
[129]	Chitosan	TiO_2	1 %	PRE	0.192 mm	/	200 μm gap	AVT	Grid	d_p = 150–200 μm	/	/	E = 0.49 MPa

placed in blue LED light to covalently cross-link PEGDA, subsequently alginate was further ionically cross-linked in the presence of $CaCl_2$, as shown in Fig. 5.

The system produced exhibited excellent mechanical properties (tensile strenght TS = 185 kPa and compressive strenght CS = 365 kPa). Dual cross-linking has previously been used in other alginate-based systems, for example in the work of Jianxing Liu et al. [113]. They produced a bioink with alginate and acrylamide (AM), containing laccase enzyme. The bioink also contained hydroxyapatite (HAP), as the organic-inorganic combination enhances the catalytic action. The system was cross-linked in the alginate part ionically using calcium ions, while AM was cross-linked covalently, to improve physiological stability. A particular system produced for 3DBP of alginate is shown in the work of Zitong Sun et al. [114]. Through coaxial extrusion-based 3D bioprinting at 360 mm/min, they generated a core-shell fiber, in which the shell was composed of alginate and the core of Polyether F127 Diacrylate. In addition, a co-culture of bacteria and microalgae was present in the shell, which ensured the bioremediation of pollutants. The system was photo-cross-linked and then transferred to $CaCl_2$ for ionical cross-linking. Another laccase-containing alginate system was realized by Yuwaporn Pinyakit et al. [115]. In detail, they produced a bioink containing dimethacrylate-functionalized Pluronic F127 (F127-DMA) and alginate, to which laccase (4 mg/l) was added, as shown in Fig. 6.

The bioink was printed at room temperature, printing speed of 6 mm/s and a flower-shaped system was produced, with a high surface area (2739.847 m^2) and complex geometry allowed by 3D printing to ensure sufficient contact time for the bioremediation process.

However, biomass immobilization is also achieved with other materials, such as hyaluronic acid (HA), a biocompatible polymer. An example is reported in the work of Manuel Schaffner et al. [116], who printed a macroporous grid based on HA and bacteria. Otherwise, Tobias Butelmann et al. [117], similarly produced a grid with 45 % infill density, immobilizing yeasts in the biocompatible and cross-linkable F127-bis-urethane methacrylate (F127-BUM).

3DBP, though, is not the only type of ink MEX used in pollutant removal systems. In fact, inks with properties suitable for such applications are often produced even without adding biomass. We refer to commonly non-biological printing processes, often termed Direct Ink Writing (DIW), which, however, have very similar characteristics to 3DBP. In some cases, absorbent properties are achieved by blending different polymers, as in the work of Abraham Samuel Finny et al. [118], in which a system containing alginate and polyethyleneimine (PEI) with heavy metal adsorption capabilities was produced. In addition, Peyman Asghartabar Kashi et al. [119] printed a robust system with hierarchical porosity based on PVA and acrylic acid (AA), in fact PVA has shown absorbent properties in aqueous systems, being hydrophilic, and AA allowed for photocross-linking. Similarly, Gayan A Appuhamillage et al. [120] previously exploited the absorbent properties of chitosan by blending it with diacrylated Pluronic F-127 (DA PluronicF-127), which allowed for UV curing after printing. Instead, Bo Xu et al. [121] produced an ink based on Cellulose nanocrystals (CNC) whose hydrophobicity was achieved by mixing with ethyl-lauroyl-arginate-hydrochloride (LAE), to improve the adsorption of CNCs at the gas-liquid interface. The ink was printed at a printing speed of

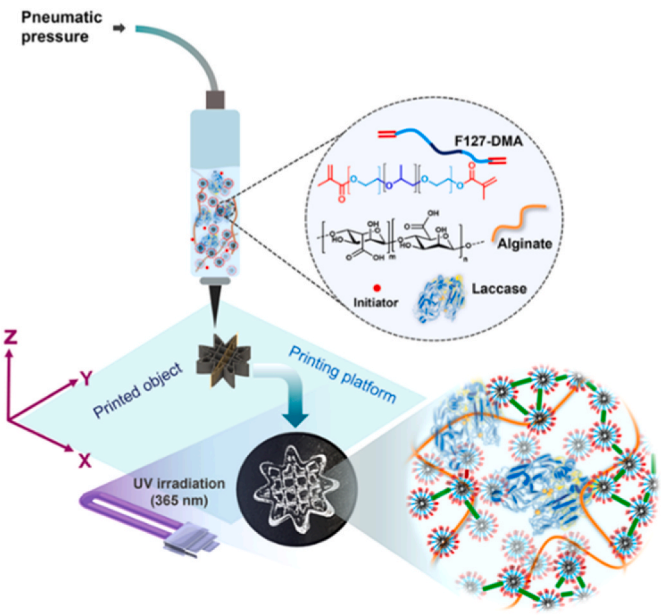

Fig. 6. Schematic Illustration for 3D printed system production, composition and shape. Reproduced with permission [115]. Copyright 2023, American Chemical Society.

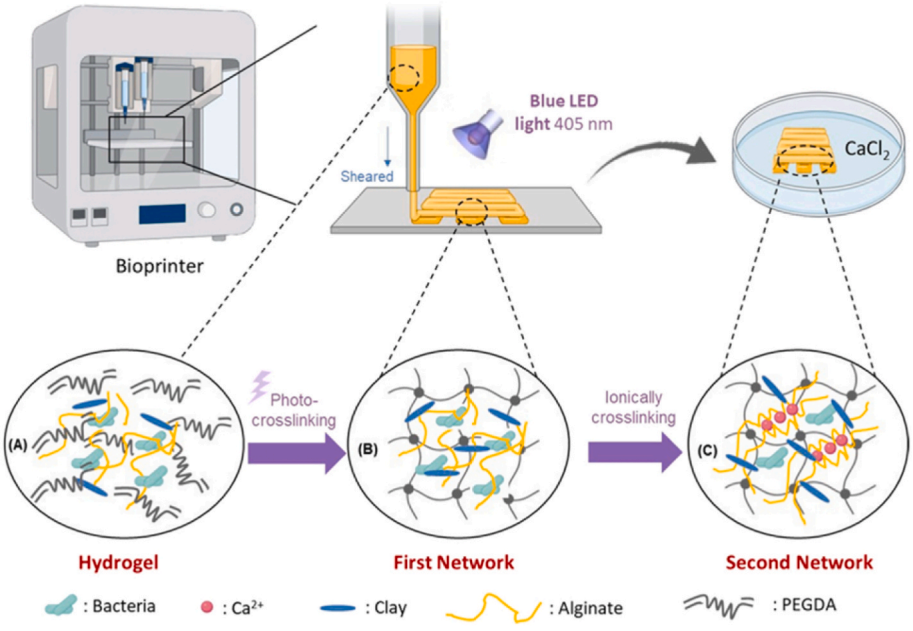

Fig. 5. Schematic illustration of 3D printing and dual cross-linking. Reproduced with permission [112]. Copyright 2022, Elsevier.

10 mm/s to generate grids with infill spacing up to 1.25 mm and high surface area.

Alternatively, various types of fillers can be incorporated in polymeric systems to provide pollutant absorption properties, as observed in Table 2. For example, Hani Nasser Abdelhamid et al. [123] created an ink by combining cellulose nanofibrils (CNF), alginate, and covalent organic frameworks (COFs) materials, where the latter exhibit high surface area and absorbent capacity. The ink was printed to create a grid with hierarchical porosity and macropores generated by the geometry, which was then ionically cross-linked in CaCl2. Metal-organic frameworks (MOFs), on the other hand, were immobilized in alginate-based ink and then printed with printing speed 33 mm/s and cross-linked in CaCl2, in the work of Rui Pei et al. [124]. The system produced is a hexagonal porous grid with a high surface area (83 m^2/g). Moreover, it had good mechanical properties, i.e. tensile strenght TS = 0.4 MPa and compressive strenght CS = 1.8 MPa. Instead, Hani Nasser Abdelhamid et al. [125] immobilized MOFs in a cellulose ink, with high loading of 67.5 wt%. The ink was then printed to create a grid with hierarchical porosity (macropores d_p = 1 mm and nanopores d_p = 20–900 nm) and high surface area.

Cellulose was also used as a matrix for 3D prining by Yang Zhang et al. [126]. They immobilized efficient adsorbent Fe3O4 26 % wt in a cellulose ink, which was then printed with a metallic nozzle (0.84 mm) at 5 mm/s. The latex-like structure produced exhibits pore volume V_P = 0.03 cm^3/g and high surface area (30 m^2/g).

Carbon-based fillers, such as GO, are also used in ink MEX-based printing. Arvid Masud et al. [127], for example, used two bio-inspired polymers, polydopamine (PDA) and bovine serum albumin (BSA) together with GO. The ink was printed from a 0.6 mm nozzle at 20 mm/s to produce a cylindrical structure that was then subjected to freeze-drying, in order to obtain a highly porous aerogel (P > 90 %). The structure had a surface area of 9.82 m^2/g. Alternatively, J.J. Moyano et al. [128] produced a system based on polyethylenimines/polyethylene glycol (PEI/PEG) and GO/silica (SiO2). In detail, the ink containing PEI/PEG and GO (4.8 % wt) was printed using a printing syringe with a needle of 0.41 mm to generate a grid scaffold with a 780 μm gap between the rods. After various intermediate treatments, the structure was covered with SiO_2 and subjected to Ammonia Vapour Treatment (AVT) curing. The hydrophilic structure showed porosity P > 94 % and surface area >190 m^2/g; it also exhibited compressive strengths CS in the range 0.1–0.4 MPa.

Titanium oxide (TiO_2) is also used in DIW processes [130], usually as pure powder or sometimes with polymeric binder [131]. For example, Laura Bergamonti et al. [129] realized TiO_2 supported chitosan scaffolds (1 % w/v) as a promising material for wastewater treatment. The ink was printed in a grid with a 200 μm gap between the rods and Young's modulus E = 0.49 MPa.

4.2. Non-Material Extrusion (non-MEX) systems

Another way to produce 3D printed systems for water pollutants removal involves the use of non-MEX systems, i.e. based on passive systems in which the device is formed from a powder (Powder Bed Fusion) or a resin (Vat Polymerization) using lasers or beams.

Processing technology, composition, printing parameters and main characteristics of polymer-based systems for water remediation recently produced by 3D non-MEX printing are listed thoroughly in Table 3.

4.2.1. Powder Bed Fusion

Systems produced by Powder Bed Fusion, i.e. Selective Laser Sintering (SLS) processes in which a solid 3D matrix is constructed by layer-by-layer sintering of hot melt material, involve the use of thermoplastic polymers, ceramics or metals, often together with fillers. Polymeric materials typically used are polyamide (PA), polypropylene (PP), but recently also polyurethane (PU), polycarbonate (PC), polyetheretherketone (PEEK), polystyrene (PS) [148].

For instance, Pengbo Sun et al. [132] produced a system by subjecting a powder of PU after mixing it with chitosan, a heavy metal capturing agent, to SLS process by a 1.5 W laser. The structure produced had hierarchical porosity and it was hydrophilic. Instead, Rui Li et al. [133] generated a 3D polyamide (PA) grid from a powder containing 10–40 % wt MOF. The laser used has a power ranging from 8.4 W to 13.2 W, and has allowed to generate a macroporous structure with an elastic modulus E varying between 15 and 40 MPa. More recently,

Table 3
Processing, composition, printing parameters and main characteristics of polymer-based systems for water remediation produced by 3D non-MEX printing recently.

Ref	Processing	Composition	Filler	Filler Conc.	Filler Imm.	Laser	Cross-linking	Shape	Porosity	SA	WCA	Mechanical Properties
[132]	SLS	Chitosan/PU	/	/	/	1.5W	/	Membrane	Hierarchical porosity	/	<90°	/
[133]	SLS	PA	MOFs	10–40 %	PRE	8.4–13.2W	/	Grid	Hierarchical porosity	/	<90°	E = 15–40 MPa
[134]	SLS	PA	TiO_2	5.4 %	POST	/	/	Prism	Hierarchical porosity	/	/	/
[135]	SLA	Resin/ Chitosan	/	/	/	/	Light	Grid	Macropores	0.254 m^2/g		
[136]	SLA	Resin	TiO_2	2 %	PRE	/	Light	FCCS	Macropores	/	/	TS = 9.98 MPa
[137]	SLA	Resin	TiO_2/SiO_2	90:5:5	PRE	/	Light	Grid	Macropores	/	/	/
[138]	SLA	Resin	PdCl2	1 %	POST	/	Light	Honeycomb monolith	P = 85 %	587 m^2/g	/	/
[139]	SLA	Resin	Graphene/ MnO_2/Fe_3O_4	0.01 g/ ml	PRE	/	Light	Graphene-like network	Macropores	/	/	/
[140]	SLA	Resin	B	/	POST	/	Light	Gyroid	Macropores	82.96 × 10^{-4} m^2	/	/
[141]	SLA	Resin	Laccase	4 %	PRE	/	Light	Ring	/	/	/	/
[142]	SLA	Resin	MOFs	/	POST	/	Light	Network of cubes	d_P = 0.8 mm	/	/	/
[143]	/	PEGDA	AgNPs	0.5 mg/ml	PRE	/	Light	Grid	Macropores	/	/	/
[144]	DLP	PEGDA	TiO_2	20 %	PRE	/	Light	Grid	Macropores	/	/	CS = 500 kPa
[145]	DLP	Resin	WO3+UiO-66+rGO	10 %	PRE	/	Light	Gyroid	Macropores	/	/	/
[146]	DLP	Resin	ZIF-8+OpdA	/	POST	/	Light	Grid	Macropores	/	/	/
[147]	DLP	Resin	MXOF	/	POST	/	Light	Lattice	P = 80 %	/	/	/

Mathieu Grandcolas et al. [134] fabricated a PA structure with SLS and then coated it with TiO_2 (5.4 % wt), taking advantage of the high surface area given by the special geometry of hexagonal prism vertex centroid, obtained by the printing technology.

4.2.2. Vat Polymerization

Among the most widely used non-MEX 3D printing techniques is vat photopolymerization, in which ultraviolet (UV) light is used to cross-link a light-curable material, without the use of high-temperature lasers. Both stereolithography (SLA) and digital light processing (DLP) processes can use commercial resins, typically acrylate-based, even with specific fillers for water remediation processes, as seen above [149]. These systems may involve the use of polymeric materials alone, as in the work of Dongxing Zhang et al. [135] in which a high surface area (0.254 m^2/g) grid was produced by SLA and then covered with chitosan absorbent, or composites with fillers.

For example, Dingyi Wang et al. [136] produced a robust macroporous face-centred cubic structure (FCCS) by SLA using a commercial resin, within which nano-sized TiO_2 (2 % wt) was embedded. Ampika Bansiddhi et al. [137] produced a similar system, using an acrylate-based resin with TiO_2 and silica (SiO2) adsorbent, with photocurable resin:SiO_2:TiO_2 composition equal to 90:5:5.

Instead, Pauline Blyweert et al. [138], made a monolith with honeycomb pattern by using a commercial tannin-based acrylate resin, on which PdCl5 was deposited post production, for catalysis processes. The porous structure exhibited P = 85 % porosity and high surface area (587 m^2/g).

Bhuvaneswari Kandasamy et al. [139] used a commercial resin with graphene/MnO_2/Fe_3O_4 catalytic fillers to produce graphene-like network systems, by combining the large surface area of graphene with the catalytic capabilities of manganese dioxide (MnO_2) and magnetite (Fe_3O_4), to achieve synergistic effects leading to increased pollutant degradation efficiency.

Biomass can also be immobilized in resins before or after the manufacturing process, for bioremediation, as observed in Table 3. For example, Gabriel Proano-Pena et al. [140] made gyroids of a few mm^3 from an acrylic resin. The structures, with a high surface area (82.96 × 10^{-4} m^2), were then inoculated with a bacteria community. Instead, Xiaoyan Xu et al. [141] made systems from PEGDA and laccase (4 % w/v) in the shape of a ring with a 5 mm central hole.

For water remediation, MOFs can also be embedded in polymer resins, or immobilized later. For example, Andreu Figuerola et al. [142] made a macroporous matrix of interconnected cubes with SLA on a resin. Subsequently, the structure was covered with ZIF-67.

Luca Burratti et al. [143] produced a macroporous grid from PEGDA resin doped with silver nanoparticles (AgNps), following the scheme shown in Fig. 7, in which light from a photo-projector is reflected by a mirror and photopolymerizes the solution layer by layer.

Similar systems can also be achieved with DLP, as previously explained. Recently, Do Hyeog Kim et al. [144] used DLP on a PEGDA-based resin with 20 % wt of TiO_2 and produced a macroporous grid with good mechanical performance (compression strength CS = 500 kPa). Vu Thi Huong et al. [145], instead, produced a ternary nanocomposite, using tungsten trioxide (WO3), MOF UiO-66 and reduced graphene oxide (rGO) to increase photocatalytic efficiency, by incorporating them into a commercial resin (10 %). The structure produced was a macroporous gyroid of 1 cm^3. Ruhani Singh et al. [146], on the other hand, produced a bioactive macroporous grid with a commercial resin for DLP and then immobilize over ZIF-8 encapsulated organophosphate degrading enzyme A (OpdA). Next, Hossein Shahriyari Far et al. [147] produced a highly porous vintiles lattice (P = 80 %); the 3D-printed lattices were then postcured and MXene/metal-organic framework (MXOF) were immobilized, where MXene is a new type nanomaterial with high surface area and tunable chemistry, used to enhance the adsorption performance of 3D-printed lattice structures.

5. Performances of 3D printed systems for water remediation

The production techniques and composition chosen for the 3D systems previously discussed imply different morphological and chemical-

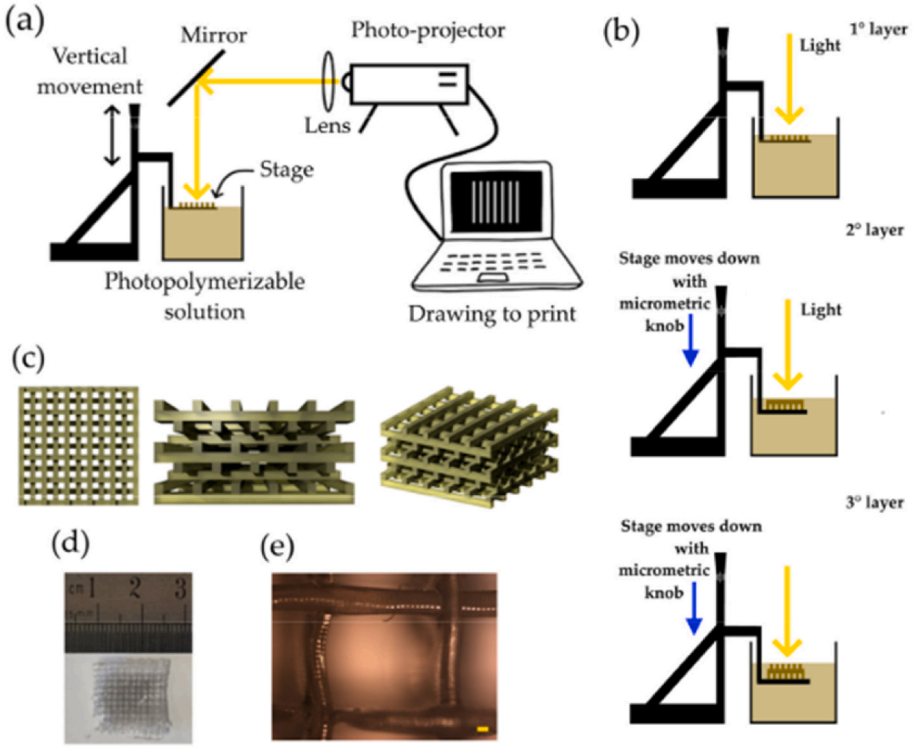

Fig. 7. (a) Schematic representation of 3D printing system, (b) working principle based on photopolymerization; (c) schematic illustrations of 3D system; (d) photo of a system; and (e) image of optical microscope. Reprinted with permission [143]. Copyright 2024, MDPI.

physical properties, as already shown; this also generates different functional performances in water pollutant removal, as the different composition of the system will allow different type of removal techniques for pollutants of various kinds; in addition, the treatment efficiency and reusability of the system will depend on the previously discussed main properties of the system, like its shape, surface area and porosity, as well as mechanical stability and wettability, which will be a consequence of the production technique. In the following paragraphs, the previously discussed systems will be analyzed in detail, examining their functional properties emerged as a result of MEX or non-MEX production and fillers inserted, in the context of removing various types of pollutants. The analysis will highlight the Removal Efficiency (R_E) for specific treatment times (t_T), the treatment for various reuse cycles, and the Removal Efficiency at the nth cycle (nth R_E), which, in the ideal life cycle of a 3D printed system for water pollutant removal, should remain very high. In particular, for each cathegory of 3D Printing, a distinction will be made between pollutant removal methods that involve their degradation or transformation, and those that involve their

Table 4
Type of removal for specific pollutants, removal efficiency at the first cycle of use and after n cycles for water remediation produced by 3D melt MEX printing recently.

Ref	Composition	Type of Removal	Type of Pollutant	Pollutant	Pollutant conc.	1st R_E	t_T	Treatment for reuse	Reusability [nth cycle]	nth R_E
[52]	PLA@TiO_2	Photodegradation	Dyes	Methyl orange	3 ppm	80 %	24h	/	/	/
[53]	PLA@TiO_2	Photodegradation	PHAs	Fluoroìanthene, pyrene, benzo(a) anthacene, chrysene, benzo(a)pyrene	3.15 μg/l, 2.40 μg/l, 0.72 μg/l, 0.82 μg/l, 0.44 μg/l	91 %, 94 %, 80 %, 54 %, 68 %	24h	/	/	/
[54]	PLA@TiO_2	Photodegradation	Dyes	Methyl orange	3 mg/l	100 %	24h	/	/	/
[55]	PLA@TiO_2	Photodegradation	Algal blooms	Microcystin	41 μg/l	100 %	24h	/	/	/
[73]	PS@TiO_2	Photodegradation	Dyes	Methylene Blue	20 ppm	98 %	60min	?	5	72 %
[74]	LDPE@TiO_2	Photodegradation	Dyes	Methyelene Blue	1 mg/dm^3	14 %	120min	/	/	/
[75]	PETG@ TiO_2/CNT	Photodegradation	Drugs	Amoxicillin	1 mg/l	Low	120min	/	/	/
[56]	PLA@ZnO	Photodegradation	Dyes	Rhodamine blue	5 mg/l	94.3 %	6h	Ultrasonication in ethanol	3	83.7 %
[57]	PLA@ ZnO/Bi_2Mo_6	Photodegradation	Dyes	Rhodamine blue	5 mg/l	99.4 %	350min	Ultrasonication in water	3	91.6 %
[56]	PLA@MOF	Photodegradation	Drugs	Ciprofloxacin	10 mg/l	>90 %	160min	/	/	/
[64]	PLA@ Carbon Nitride	Photodegradation	Drugs	VFX	5 mg/l	90 %	60min	Washed in distilled water	5	90 %
[59]	PLA@Fe_3O_4	Catalyst	Drugs	Ofloxacin	1 mg/l	82 %	3h	/	/	/
[66]	PLA@ Laccase	Biocatalyst	Drugs	E2, EE2	356 ng/L, 187 ng/L	40 %, 35 %	24h	Washed in acetate buffer	5	10 %–20 %
[76]	PETG/PVA	Adsorption	Drugs	NSAIDs	1 mg/ml	80 %	4h	/	/	/
[81]	PCL/SA	Adsorption	Heavy metals	Cu^{2+}	0.17 %	22.8 %	30days	/	/	/
[58]	PLA@Fe_3O_4	Adsorption	Heavy Metals	Arsenic	20 mg/l	96.2 %	5h	Washed in acid solution	3	77 %
[60]	PLA@ TCNFs/MOF	Adsorption	Heavy Metals	Mn^{2+}	Real Wastewater	57 %	24h	Immersion in NH_4Cl, treatment with HCl, re-anchoring	3	49.2 %
[61]	PLA@ GO/Chitosan	Adsorption	Dyes	Crystal Violet	50 mg/l	97.8 %	120min	/	/	/
[62]	PLA@GO	Adsorption	Heavy metals	Cd, Pb	10 mg/l	>90 %	120min	Washed in diluted acid	5	60 %
[63]	PLA@ Carbon Black	Adsorption	VOC	Benzene, Toluene, Ethyl-benzene	105 ppm, 104 ppm, 103 ppm	50.6 %, 81.3 %,92 %	5h	/	/	/
[65]	PLA@MA	Bioadsorption	Chemicals, biologicals	Nitrogen, phosporus, bacteria	Real wastewater	90 %, 85 %	5days	/	/	/
[67]	PLA/ PBAT@MA	Bioadsorption	Dyes	Methylene Blue	100 mg/l	92.66 %	24h	Washed in HCl	6	72 %
[68]	PLA@Zeolite	Adsorption	Chemicals	Ammonia	1 mg/l	65 %	48h	/	/	/
[69]	PLA@Zeolite	Adsorption	Chemicals	Ammonia	44 mg/l	83 %	48h	/	/	/
[70]	PLA@HAP	Adsorption	Heavy metals	Cd, Pb	5 ppm	45 %, 40 %	12h	/	/	/
[71]	PLA/PBS/ PVA@CSP	Adsorption	Dyes	Methylene Blue	100 mg/l	89.84 %	72h	Washed in ethanol	7	Slight decline
[72]	PLA@ TCNF, ChNF	Adsorption	Heavy metals	Cu^{2+}	1 mM	47 %, 51 %	8h	Washed in HCl	3	>20 %
[82]	MB@ SLP/NPK	Adsorption	Heavy metals	Cu^{2+}	1000 mg/l	78 %	30days	/	/	/
[77]	ABS@ZnO	Extraction	Dyes	Malachite Green	5 mg/l	99 %	5h	Washed in etahnol	7	50 %
[78]	ABS/TPU@ $CaSiO_3$	Adsorption	Dyes	Methylene Blue	50 mg/l	88 %	5h	Ultrasonication in methanol	6	70 %
[79]	ABS@POM	Adsorption	Heavy metals	Cu^{2+}, Ni^{2+}, Co^{2+}	2.2 mM	67.1 %, 44.2 %, 40.5 %	12h	/	/	/
[80]	PA@ Carbon Fiber	Extraction	Pesticides	OCPs, OPPs	100 μg/l	100 %	120min	Washed in acetonitrile	10	100 %

isolation and separation from aqueous solution.

5.1. Material Extrusion (MEX) systems

5.1.1. Melt MEX systems

Table 4 will discuss in detail the types of removal for specific pollutants, the removal efficiency at the first cycle of use and after various cycles, for systems produced by 3D melt MEX printing.

5.1.1.1. Pollutants degradation and transformation. Pollutant degradation refers to a series of chemical and biological processes through which harmful substances are transformed into less harmful or completely harmless compounds. These processes can be driven by light (photodegradation), chemical reactions (catalyst), biological activity (biocatalyst and bioremediation), and are essential for reducing the environmental impact of pollutants.

In systems containing TiO_2, photocatalytic filler, the main mechanism of pollutant removal is photodegradation. For example, in the PLA@TiO_2 system produced by Pablo Ortega-Columbrans et al. [52] photodegradation was the removal mechanism for the methyl orange dye; specifically, starting from a 3 ppm aqueous solution of pollutant, they achieved 80 % removal efficiency R_E in 24h.

Similarly, Sangiorgi et al. [54] made a comparable system, but with a higher concentration of TiO_2, that produced methyl orange R_E (3 mg/l) of 100 % in 24h.

Photodegradation activity was also obtained in the similar system of Andrew D. McQueen et al. [53], in this case targeting complex aqueous mixture of organic contaminant compounds, namely Polycyclic Aromatic Hydrocarbons (PAHs). Various substances of this type in aqueous solution with concentration in the order of μg/l were removed with R_E up to 94 % in 24h.

Alan J. Kennedy et al. [55], on the other hand, used photodegradation to remove harmful microcystin algal toxin. Specifically, starting from a solution with 41 μg/l of pollutant, they achieved 100 % R_E in 24 h.

Previous systems have been realized in PLA, but, as formerly explained, melt MEX 3D printing by inserting TiO_2 as a filler is also used with other materials. For example, the PS@TiO_2 based system of Viskadourakis et al. [73] provided a methylene blue dye (20 ppm) removal efficiency of 98 % in 60 min. In addition, the system is reused for 5 cycles, and at the 5th cycle R_E is 72 %. However, it is often difficult to achieve high removal efficiencies using other polymers because it complicates the processing of material with high filler content and the possibility of obtaining high surface area structures. For example, the LDPE@TiO_2 system made by María J. Martín de Vidales et al. [74] removed only 14 % methylene blue (1 mg/dm^3) in 120 min. Low R_E was also obtained in the PETG@TiO_2/CNT system of Kristina Miklec et al. [75] in the removal of Amoxicillin (1 mg/l) in 120 min.

Photodegradation of pollutants also occurs using ZnO as a filler. For example, Kun Li et al. [56] produced a PLA@ZnO system for the photodegradation of rhodamine blue dye. The system was used in an aqueous solution with 5 mg/l pollutant; in 6 h the removal efficiency R_E was 94.3 %. The stability of the system was tested by reusing it for three cycles with intermediate ethanol ultrasonications, maintaining an R_E at the last cycle of 83.7 %. In the same work, the authors produced a PLA@MOF system by exploiting the photocatalytic potential of the iron-based metal organic framework for the removal of the ciprofloxacin (10 mg/l) achieving R_E >90 % in 160 min. The same authors in another work [57], achieved better performance in removing the rhodamine blue dye using their PLA@ZnOBi$_2$MoO$_6$ system, where bismuth molybdate (Bi_2MoO_6) enhanced photocatalytic activities. In fact, R_E equal to 99.4 % was achieved in 350 min. Moreover, R_E was maintained at 91.6 % after three cycles of reuse.

Photocatalytic activity has also been exploited by Manuel Peñas-Garzón et al. [64] in their PLA@Carbon Nitride photocatalyst, for removing the venlafaxine (VFX). Specifically, 90 % of VFX was removed in 60 min from an aqueous solution with 5 mg/l pollutant. In addition, the system was used for 5 cycles by washing it in distilled water, without observing reductions in R_E.

S. Fernandez-Velayos et al. [59], instead, exploited chemical catalysis resulting from sodium persulfate activation for ofloxacin degradation, using their PLA@Fe_3O_4 system; in 3 h, 82 % drug was removed from an aqueous solution with 1 mg/l pollutant. Finally, the system of Agnieszka Rybarczyk et al. [66] provided catalytic degradation promoted by laccase enzyme (biocatalysis), of estrogens 17α-ethynylestradiol (EE2) and 17β-estradiol (E2). Specifically, starting from aqueous solutions with concentrations of 356 ng/L and 187 ng/L, respectively, removal efficiencies of 40 % and 35 % in 24 h were obtained. The system was reused for 5 cycles, with intermediate washes in acetate buffer, and R_E drops, ranging between 10 % and 20 %.

5.1.1.2. Pollutants isolation. More commonly, pollutants removal methods do not involve their degradation, but their isolation from aqueous solutions, usually by adsorption processes: in these cases, the pollutant interacts with the 3D system and it is separated from the remaining solution, without undergoing transformation of any kind.

In some cases, the adsorptive sites of the polymer matrix are directly exploited to remove pollutants. For example, Ankur Jyoti Thakuria et al. [76] exploited the active sites of PETG in their 3D system, to adsorb non-steroidal anti-inflammatory drugs (NSAIDs), achieving R_E of 80 %. Alternatively, Ioannis L. Liakos et al. [81] exploited their PCL/Alg system for adsorption of Cu^{2+} copper ions, obtaining low R_E.

However, fillers are frequently inserted for enhancig the ability of 3D systems to remove pollutants. For example, the PLA@Fe3O4 system by Kihoon Kim et al. [58] provided adsorption of the heavy metal arsenic from a 50 mg/l solution. R_E was equal to 96 % after the first use, and became 77 % after 3 cycles with strong acid solution washes and re-deposition of iron(III) oxide.

G. Zhou et al. [61], on the other hand, exploited the adsorptive properties of GO and Chitosan for adsorption of the crystal violet dye through their 3D PLA@GO/Chitosan system. Specifically, the system removed 97.8 % pollutant from an aqueous solution (50 mg/l) in 120 min. Instead, the PLA@GO system by Sung-Sil Park et al. [62] was used for adsorption of heavy metals, such as cadmium (Cd) and lead (Pb). Specifically, they achieved R_E >90 % in 120 min for 10 mg/l solutions.

Lagalante et al. [63] produced a PLA@Carbon Black system, exploiting the water cleanup properties of the filler, for the adsorption of volatile organic compounds (VOCs) from water, such as benzene, toluene, and ethyl benzene, from solutions with concentrations of 105 ppm, 104 ppm, 103 ppm, respectively. In 5 h, R_E of 50.6 %, 81.3 %, 92 % were obtained, respectively.

Adsorption processes can also be stimulated by biomass such as microalgae (MA), referring to the process as bioadsorption. For example, the PLA@MA system by Patricia Laura Marcon et al. [65] was used to bioadsorb phosphorus and nitrogen species, and pathogenic bacteria, from real wastewater. Specifically, they achieved removal efficiency of 90 % of chemical species and 80 % of biological species in 5 days. In contrast, Xinshu Xia et al. [67] made a PLA/PBAT@MA system for methylene blue bioadsorption. Starting from a 100 mg/l solution, they removed 92.66 % in 24 h. In addition, washes in hydrochloric acid (HCl) allowed for reuse of the system for 6 cycles, with R_E at the last cycle of 72 %.

Alan J. Kennedy et al. [68], in addition, used zeolite-containing systems to treat ammonia contaminated water. Specifically, they produced PLA@Zeolite system that was used to treat water with 1 mg/l of ammonia, achieving R_E of 65 % in 48 h. Later, they produced a PLA@Zeolite system increasing the filler content [69], achieving R_E of 83 % in 48 h from solutions with ammonia concentration of 44 mg/l. Instead, Natalia Fijoł et al. [70] removed heavy metals using a PLA@-HAP system. Specifically, they removed Cd and Pb from aqueous

solutions 5 ppm, with removal efficiencies of 45 % and 40 %, respectively, in 12 h.

Adsorptive properties are also enhanced by natural fillers. For example, Yinglian Zheng et al. [71] adsorbed methylene blue using a PLA/PBS/PVA@CSP system, where camellia seed powder (CSP) provided sites for dye adsorption, which may involve hydrogen bonding, electrostatic attraction and other types of multiple interactions, as shown in Fig. 8.

In detail, they obtained R_E of 89.84 % from aqueous solution with 100 mg/l pollutant in 72 h. The system was washed in ethanol and reused for 7 cycles, they observed a slight decline in efficiency. In parallel, the 3D system in PLA and TCNF or ChNF by Natalia Fijoł et al. [72] exploited cellulose and chitin fibers to adsorb copper ions (Cu^{2+}) from 1 mM aqueous solutions, achieving R_E of 47 % and 51 %, respectively. After three cycles of use and washes in HCl, R_E decreased by more than half for both. In addition, Scaffaro et al. [82] exploited the active sites of NPK fertilizer flour and tomato plant waste particles (Solanum Lycopersicum, SLP) in the MB@SLP/NPK system to adsorb Cu^{2+} copper ions. Specifically, they obtained R_E of 78 % in 30 days, starting from solutions with 1000 mg/l concentration.

Instead, Sidra Waheed et al. [77] used their ABS@ZnO system to perform in-situ growth of a type of metal-organic frameworks (ZIF-8), as previously explained: the filler had adsorptive properties, which ensured extraction of the pollutant malachite green dye (5 mg/l) with R_E of 99 % in 5 h. In addition, the system was reused for 7 cycles, with intermediate washes in ethanol and final R_E equal to 50 %. Similarly, Zhen Liu et al. [78] performed in Situ Growth of Ca^{2+} based metal-organic Framework on ABS/TPU@$CaSiO_3$ 3D system for methylene blue (50 mg/l) adsorption. R_E achieved 88 % in 5 h and it was maintained at 70 % after 6 cycles of reuse and ultrasonication in methanol.

Yuanchun Ji et al. [79] used polyoxometalate (POM) anions as heavy metal binding sites. Specifically, their ABS@POM system adsorbed copper, nickel, and cobalt ions (Cu^{2+}, Ni^{2+}, Co^{2+}) from 2.2 mM aqueous solutions, with R_E of 67.1 %, 44.2 %, 40.5 % in 12 h, respectively.

Recently, Camila Scheid et al. [80] used PA@Carbon fiber system to remove organochlorine pesticides (OCPs) and organophosphorus pesticides (OPPs), achieving RE 100 % in 120 min from solutions with pollutant concentration 100 μg/l. In addition, the system was reused for 10 cycles without exhibiting loss of efficiency.

5.1.2. Ink MEX systems

Table 5 will discuss in detail the types of removal for specific pollutants, the removal efficiency at the first cycle of use, and after various cycles, for systems produced by 3D ink MEX printing.

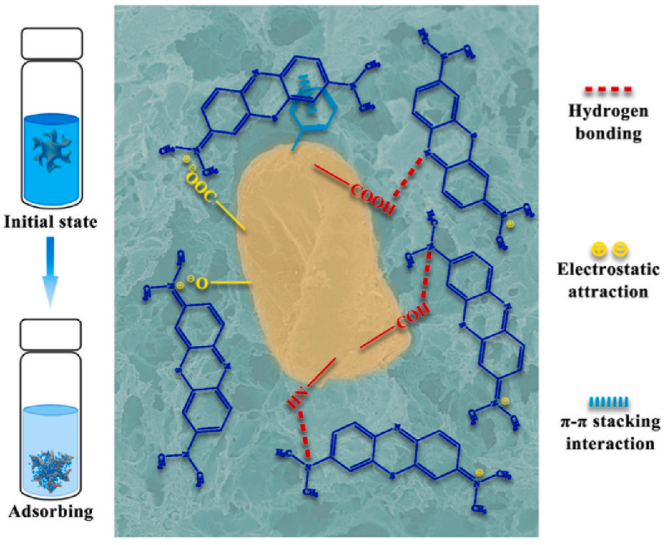

Fig. 8. Possible adsorption mechanism of methylene blue on PLA/PBS/PVA@CSP system. Reproduced with permission [71]. Copyright 2021, Elsevier.

5.1.2.1. Pollutants degradation and transformation. In the category of ink MEX 3D printed systems, the removal of pollutants by degradation is predominantly a biological process guaranteed by the presence of bacteria or enzymes (bioremediation or biocatalysis, respectively); in fact, for this type of production, incorporating biomasses and ensuring their activity, is easier than in melting processes, as mentioned in the previous paragraphs.

For istance, Yan Li et al. [112] exploited the bioremediation action produced by bacteria (B) in their PEGDA/Alg/PVA@n-clay,B 3D system for ammonia removal, achieving R_E nearly 100 % in 72 h. The system was reused for 3 cycles without losing efficiency. High R_E was also previously obtained by bioremediation of phenolic compounds, by using HA@B system of Manuel Schaffner et al. [116]. Specifically, starting from a concentrated solution (400 mg/l), complete removal of the pollutant was achieved in 135 h.

More recently, Zitong Sun et al. [114] incorporated an algal-bacteria consortium into an Alg/F127-DA system for methyl orange bioremediation, achieving RE 90 % in 48 h. In addition, the system was reused for 4 cycles without intermediate treatment, reducing RE to 43 %. Alternatively to bioremediation, in this category we also find systems used for biocatalysis, usually by enzyme laccase. For example, Jianxing Liu et al. [113] used their system in Alg/AM@HAP,Laccase, to degrade chlorophenol from 10 mg/ml aqueous solutions. R_E of 80 % in 24 h was obtained. In addition, the system was reusable for 7 cycles, with intermediate washes in deionized water.

Instead, the 3D F127-DMA/Alg@Laccase system by Yuwaporn Pinyakit et al. [115] was used to degrade orange(II) from solutions with 25 ppm pollutant concentration. R_E of 100 % was obtained in 60 min. In addition, the system was reusable for 7 cycles, maintaining R_E at 50 %.

Alternatively, ink MEX printed systems are also used for photocatalytic processes, tipically by adding TiO_2 as a filler. For example, Chitosan@TiO_2 system produced by Laura Bergamonti et al. [129] was used to degrade the antibiotic amoxicillin, achieving 100 % removal in 120 min. Instead, recently, Hani Nasser Abdelhamid et al. [125] used their Cellulose@MOFs system to catalytically degrade methylene blue and adsorb cobalt ions (CO^{2+}), achieving complete dye removal in 10 min and high adsorption capacities for the heavy metal in 12 h.

5.1.2.2. Pollutants isolation. In the context of ink MEX systems that ensure the isolation of pollutants by exploiting the active sites of the polymer matrix, Abraham Samuel Finny et al. [118] proposed the Alg/Gelatin/PEI system for the adsorption of copper ions (Cu^{2+}), achieving a removal efficiency R_E of 98 % in 18 h. Peyman Asghartabar Kashi et al. [119], on the other hand, used their PVA/AA system for the removal of lead ions (Pb^{2+}) with good adsorption capacity in few minutes. Gayan A Appuhamillage et al. [120] also focused on the removal of metal ions with the Chitosan/DAPluronic F-127 system, capable of up to 95 % metal removal in 30 min from 3000 ppb stock solutions. Recently, Bo Xu et al. [121], developed a CNC/LAE system for the adsorption of microplastics. Specifically, they removed polystyrene (PS) microspheres from aqueous solutions (0.10 mg/ml), achieving an adsorption capacity of 300 mg/g in 210 min.

Also in this category, immobilization of biomass such as microalgae (MA) ensures bioadsorption processes. For example, Seon-Won Yoon et al. [109] exploited their Alg/MC@MA 3D system that efficiently absorbs nitrogen and phosphorus; in particular, starting from aqueous solutions with concentrations of 23.6 mg/l and 2.11 mg/l, respectively, they achieved R_E of 52 % and 88 % in treatment times t_T of 15 days.

Mahdiyar Shahbazi et al. [122], instead, exploited the filler in their Alg/AA@n-clay system to enhance the adsorption abilities of lead ions Pb^{2+} from aqueous solutions (500 mg/l), with good adsorption capacity.

Covalent Organic Frameworks (COFs) are also often used, as in the

Table 5
Type of removal for specific pollutants, removal efficiency at the first cycle of use and after n cycles for water remediation produced by 3D ink MEX printing recently.

Ref	Composition	Type of Removal	Type of Pollutant	Pollutant	Pollutant conc.	1st R_E	t_T	Treatment for reuse	Reusability [nth cycle]	nth R_E
[112]	PEGDA/Alg/PVA@n-clay,B	Bioremediation	Chemicals	Ammonia	70 mg/l	≈100 %	72h	/	3	≈100 %
[116]	HA@B	Bioremediation	Phenolics	Phenol	400 mg/l	100 %	135h	/	/	/
[114]	Alg/F127-DA@Algal-B	Bioremediation	Dyes	Methtyl orange	10 mg/l	90 %	48h	/	4	43 %
[113]	Alg/AM@HAP,Laccase	Biocatalyst	Phenolics	Chlorophenol	10 mg/ml	80 %	24h	Washed in deionized water	7	≈40 %
[115]	F127-DMA/Alg@Laccase	Biocatalyst	Dyes	Orange(II)	25 ppm	100 %	60min	/	7	50 %
[129]	Chitosan@TiO_2	Photodegradation	Drugs	Amoxicillin	/	100 %	120min	Washed in distilled water	3	80 %
[125]	Cellulose@MOFs	Catalyst, adsorption	Dyes, heavy metals	Methylene Blue, Co^{2+}	1 mg/ml, 500 ppm	>99 %, 328 mg/g	10min, 12h	/	/	/
[118]	Alg/Gelatin/PEI	Adsorption	Heavy metals	Cu^{2+}	100 ppm	98 %	18h	/	/	/
[119]	PVA/AA	Adsorption	Heavy metals	Pb(II)	500 mg/l	700–800 mg/g	10min	/	/	/
[120]	Chitosan/DAPluronic F-127	Adsorption	Heavy metals	Cu^{2+}, Cd^{2+}, Pb^{2+}, Hg^{2+}	3000 ppb	95 %	30 min	/	/	/
[121]	CNC/LAE	Adsorption	Microplastics	PS	0.10 mg/ml	300 mg/g	210min	/	/	/
[109]	Alg/MC@MA	Bioadsorption	Chemicals	Nitrogen, phosphorus	23.6 mg/l, 2.11 mg/l	52 %, 88 %	15days	/	/	/
[122]	Alg/AA@ n-clay	Adsorption	Heavy metals	Pb^{2+}	500 mg/l	500 mg/g	60 min	/	/	/
[123]	CNF/Alg@COFs	Adsorption	Heavy metals	Cu^{2+}	100 ppm	90 %	180min	Soaked in HCl	3	No decline
[124]	Alg/Gelatin@MOFs	Adsorption	Dyes	Methylene Blue	20 ppm	99.8 %	20min	Washed in HCl	10	82 %
[126]	Cellulose@Fe_3O_4	Adsorption	Dyes	Methylene Blue	5.6 mg/l	88.5 %	60s	Acid washing	3	85.7 %
[127]	PDA/BSA@GO	Adsorption	Heavy metals, dyes	Cr(VI), Pb(VI), methylene blue	25 ppm, 200 ppm	>93 %, >99.17 %	96h	Washed in ethanol	3	95 %

CNF/Alg@COFs system of Hani Nasser Abdelhamid et al. [123], capable of remove Cu^{2+} ions from aqueous solutions with 100 ppm concentration, achieving good adsorption capacities in 180 min. In addition, the system was suitable to be reused for 3 cycles with intermediate HCl washes, obtaining slight decline in performance. Instead, Rui Pei et al. [124] Alg/Gelatin@MOFs system exploited metal-organic frameworks (MOFs) to enhance methylene blue adsorption, achieving R_E of 99.8 % in 20 min from aqueous solutions with 20 ppm concentration. Moreover, the system was notably stable; in fact, it has been used for 10 cycles, with washes in HCl for regeneration processes as shown in Fig. 9, and R_E was reduced at 82 %.

Yang Zhang et al. [126] produced magnetic cellulose-based system containing Fe_3O_4 nanoparticles as ideal adsorbents for removing organic dyes from water. In fact, the 3D Cellulose@Fe3O4 removed methylene blue, with R_E 88.5 % in just 60 s. In addition, R_E remained nearly the same after 3 cycles of use.

Finally, Arvid Masud et al. [127] exploited graphene oxide (GO), producing a PDA/BSA@GO system to remove organic dyes and heavy metals. Specifically, they removed methylene blue (200 ppm) with R_E >99.17 %, and chromium ions Cr(VI) and lead Pb(VI) (20 ppm), with R_E >93 %. The system was tested positively for multiple cycles of dye removal, by performing ethanol washes.

5.2. Non-Material Extrusion (non-MEX) systems

Table 6 will discuss in detail the types of removal for specific pollutants, the removal efficiency at the first cycle of use, and after various cycles, for systems produced by 3D non-MEX printing.

5.2.1. Pollutants degradation and transformation

In the category of 3D systems produced by non-MEX processes and intended for the degradation of pollutants, the presence of fillers capable of ensuring photodegradative processes is prevalent. For instance, Mathieu Grandcolas et al. [134] emploied the photocatalytic activity of TiO_2 in the PA@TiO_2 system for the degradation of methylene blue from aqueous solutions with 10 mg/l concentration. They obtained R_E 94.1 % in 180 min. Similarly, Do Hyeog Kim et al. [144] photodegraded the same pollutant, using a PEGDA@TiO_2 system. In this case, they almost completely removed the pollutant in 6 h from solutions with 10 mol/l concentration. Instead, Ampika Bansiddhi et al. [137] produced a Resin@TiO_2/SiO_2 3D system, exploiting the synergy between the adsorption property of SiO_2 and photocatalytic behavior of TiO_2, to degrade the

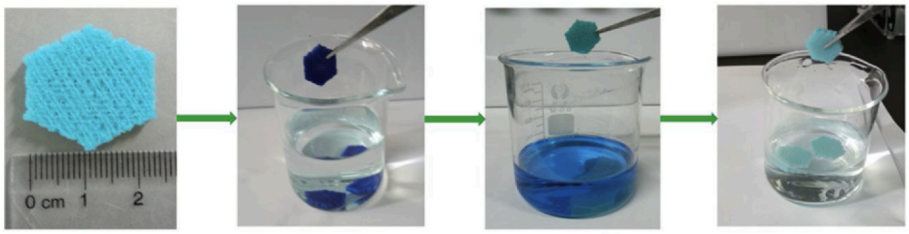

Fig. 9. Recyclability of the Alg/Gelatin@MOFs 3D system: regeneration process of adsorbents by washing in dilute HCl solution. Reproduced with permission [124]. Copyright 2020, Elsevier.

Table 6
Type of removal for specific pollutants, removal efficiency at the first cycle of use and after n cycles for water remediation produced by 3D non-MEX printing recently.

Ref	Composition	Type of Removal	Type of Pollutant	Pollutant	Pollutant conc.	1st R_E	t_T	Treatment for reuse	Reusability [nth cycle]	nth R_E
[134]	PA@TiO_2	Photodegradation	Dyes	Methylene Blue	10 mg/l	94.1 %	180min	/	/	/
[144]	PEGDA@ TiO_2	Photodegradation	Dyes	Methylene Blue	10 mol/l	≈ 100 %	6h	/	/	/
[137]	Resin@ TiO_2/SiO_2	Adsorption and photodegradation	Dyes	Methylene Blue, Rhodamine Blue	5 mg/l	81.9 %, 60 %	8h	Washed in hydrogen peroxide	3	≈ 70 %, 50 %
[145]	Resin@ WO_3+UiO-66+rGO	Photodegradation	Drugs	SMX	20 mg/l	≈ 90 %	60min	Washed in ethanol	10	Slight decline
[139]	Resin@ Graphene/ MnO_2/Fe_3O_4	Photodegradation	Dyes	Methylene Blue	110 ppm	95.5 %	120min	/	10	93.5 %
[138]	Resin@ $PdCl_2$	Catalyst	Chemicals	Oxalic Acid, Bromate	1 mM, 200 ppb	25 %, 45 %	/	/	/	/
[142]	Resin@ MOFs	Catalyst	Dyes	Rhodamine Blue	5 mg/l	100 %	10min	Washed with water	10	98 %
[146]	Resin@ ZIF-8+OpdA	Biocatalyst, adsorption	Pesicides, Heavy metals	Methyl Parathion, Cu(II)	0.2 mM, 200 ppm	57.9 % 42 %	10 min, 40min	/	/	/
[141]	PEGDA@ Laccase	Biocatalyst	Drugs	Diclofenac, Ethinylestradiol	2.5 mg/l	95 %	24h, 2h	Washed in distilled water	18	/
[132]	Chitosan/PU	Adsorption	Heavy metals	Cu^{2+}, Pb^{2+}	1000 mg/l	19.6 mg/g,30.4 mg/g	5h	/	/	/
[135]	Chitosan/ Resin	Adsorption	Heavy metals	Cu(II)	100 mg/l	>95 %	120min	Desorption with EDTA	5	Slight decline
[133]	PA@MOFs	Adsorption	Dyes	Methylene Blue	5 ppm	>90 %	24h	Washed in methanol	5	80 %
[147]	Resin@ MXOFs	Adsorption	Dyes	Methyl orange, Direct red	30 ppm	91.98 %, 84.9 %	1h	Washed in ethanol/acetone	4	90 %, 70 %
[136]	Resin@TiO_2	Adsorption	Heavy metals	As(III)	100 μg/l	99.67 %	24h	Centrifugation in NaOH	10	Slight decline
[143]	PEGDA@ AgNPs	Adsorption	Heavy metals	Hg(II)	8 mg/l	94 %	8h	/	/	/

dyes methylene blue and rhodamine blue. Specifically, starting from solutions containing 5 mg/l, they obtained R_E of 81.9 % and 60 % in 8 h, respectively. After hydrogen peroxide treatments, they reused the system for 3 cycles, with nearly 10 % decrease in R_E.

Recently, Vu Thi Huong et al. [145] produced a ternary nanocomposite 3D system Resin@WO3+UiO-66+rGO with photocatalytic activities for the degradation of the antibiotic sulfamethoxazole (SMX) from aqueous solutions with 20 mg/l concentration. They achieved R_E of 90 % in 60 min, and the system was reusable for 10 cycles without loss of efficiency. Similarly, Bhuvaneswari Kandasamy et al. [139] used a Resin@Graphene/MnO_2/Fe_3O_4 system for the photodegradation of 10 ppm of methylene blue dye. Specifically, 95.5 % pollutant was degraded in 120 min. In addition, the system was reused for 10 cycles, with final R_E of 93.5 %, proving cyclic stability.

Instead, Pauline Blyweert et al. [138] replaced photodegradation with a chemical catalytic degradation process with tannin-based resin@PdCl2, to test them as catalysts for oxalic acid oxidation and bromate reduction, achieving a 25 % transformation of the former and 45 % reduction of the latter. The Resin@MOFs system by Andreu Figuerola et al. [142] was also used for chemical-activated catalytic processes for the degradation of organic dyes (rhodamine blue) in water. Specifically, starting from solution with dye concentration 5 mg/l, a complete degradation of the pollutant was achieved in 10 min. In addition, the system showed excellent reusability up to 10 cycles, with R_E at the 10th cycle 98 %.

Ruhani Singh et al. [146] also produced a system by incorporating a type of MOFs capable of encapsulating organophosphate biodegrading enzyme (OpdA). Specifically, the Resin@ZIF-8+OpdA system was capable of degrading pesticides (methyl parathion) (57.9 %) and adsorbing Cu^{2+} copper ions (42 %). The biocatalytic process, was also promoted by the PEGDA@Laccase system of Xiaoyan Xu et al. [141] which degraded diclofenac and ethinylestradiol from aqueous solutions with concentration 2.5 mg/l, with R_E 95 % within 24 and 2 h, respectively. In addition, the system was reused for 18 cycles to evaluate enzymatic stability, via oxidation of the test substrate 2,2′-azino-bis (3-ethylbenzthiazoline-6-sulphonic acid) (ABTS).

5.2.2. Pollutants isolation

In the category of non-MEX systems produced for pollutants isolation, there is the possibility of exploiting the adsorptive sites in the matrix, as well. For instance, Pengbo Sun et al. [132] produced a Chitosan/PU system, exploiting natural adsorptive properties for Cu^{2+} copper ions and Pb^{2+} lead removal, achieving good adsorption capacities. Similarly, Dongxing Zhang et al. [135] exploited the properties of chitosan in a 3D system intended for the removal of Cu^{2+} copper ions, from aqueous solutions with 100 mg/l concentration. They obtained R_E >95 % in treatment time of 120 min. They also showed that ethylenediaminetetraacetic acid (EDTA) can desorb metal ions from the surface of the system, ensuring high efficiencies even for successive cycles of use (up to 5 cycles).

Adsorptive properties can be enhanced with fillers, as observed above. Rui Li et al. [133] used PA@MOFs system for adsorption of methylene blue from 5 ppm aqueous solutions, achieving R_E >90 % in 24 h. In addition, the system was reusable for 5 cycles with intermediate washes in ethanol, achieving R_E at the 5th cycle equal to 80 %. Hossein Shahriyari Far et al. [147] similarly used their Resin@MXOFs system, exploiting a modified version of MOFs with MXene, to adsorb methyl orange and direct red, from 30 ppm aqueous solutions. They obtained R_E of 91.98 % and 84.9 % in 1 h, respectively. In addition, the system was reusable up to 4 cycles (4th R_E equal to 90 % and 70 %, respectively), by washing it in ethanol/acetone.

Dingyi Wang et al. [136], on the other hand, made 3D Resin@TiO_2 systems for adsorption removal of arsenic As(III) in water, achieving in 24 h R_E equal to 99.67 %. The system was reusable, by performing

centrifugation in sodium hydroxide (NaOH), with no significant reduction in R_E at the 10th cycle. Recently, Burratti et al. [143] used their PEGDA@AgNPs system to adsorb Hg(II) mercury ions from 8 mg/l aqueous solutions. They obtained R_E 94 % in 8 h.

6. Discussion

The analysis conducted so far on parameters and performance of 3D systems highlights the usefulness of a trasversal comparison to evaluate the results.

When comparing various 3D manufacturing methods, melt-MEX systems are the easiest to use and the most popular due to their accessibility and simplicity of operation. Indeed, it is notable that most of the work in the literature in this regard fits into the melt-MEX category: considering the extreme prevalence of such technologies in various application fields, it is not surprising that it also plays a major role in water purification. Melt-MEX technology makes it possible to obtain various types of architectures quickly and easily, by using a large class of polymeric materials and by appropriately varying the printing parameters. As it turned out, the most widely used material is PLA, as it is very suitable for melt-MEX 3D printing processes. Fillers of various types can be added to these systems, which enhance pollutant removal capabilities, such as degradation or isolation. In general, the removal efficiency is high and the systems are used for multiple cycles. These possibilities are ensured by the high surface area and architecture of the system, which allow high contact times between absorbent and pollutant; in addition, the three-dimensionality and mechanical stability of the structure allow easy recovery of the structure and recycling possibilities, as observed.

However, in this category, manufacturing processes are usually performed at high temperatures, which can lead to problems, such as thermal degradation of sensitive materials or fillers. In addition, the incorporation of fillers PRE printing is limited to low concentrations, given the expected rheological complexity of the produced composite. In fact, POST production filler immobilization is often used, which is a simpler process, but it is more complex to accurately determine the amount of immobilized filler and filler leaching can occur.

On the other hand, ink-MEX systems operate at lower temperatures, allowing the use of different materials, often natural polymers, tipically alginate-based, with adsorptive properties, and ensures the facilitated incorporation of biomass for bioremediation processes, but with slightly greater complexity in process management, for the accuracy required in ink production and robust cross-linking processes.

Finally, non-MEX 3D printing, despite its good performance in the field of pollutant removal, is still a niche area in its use with polymer powders and resins, as it is limited to specific materials and the process is more complex to manage.

All the 3D systems analyzed provide good functional performance, which could be enhanced further. In fact, all of the systems produced enable the removal of various types of pollutants with high levels of efficiency, even over several cycles, with differences in terms of the type of removal, related mainly to the kind of filler incorporated and the properties of the material.

7. Conclusions and future perspectives

The increasing severity of water pollution requires innovative and efficient solutions for its mitigation. In this context, the use of polymeric 3D systems for the removal of aqueous pollutants has emerged as particularly promising and, therefore, much explored in recent years. These systems offer numerous advantages over traditional 2D or 1D systems, including ease of production, versatility and greater long-term mechanical stability. In addition, additive manufacturing process ensures the production of complex, highly porous, high surface area geometries that can provide higher performance in pollutant removal; in fact, peculiar architectures were produced, sometimes biomimetic, in the shape of flowers, hourglasses, grids with different types of patterns, demonstrating enormous processing versatility. Important to note that these geometries are hardly achievable by traditional methods and in any case, would not have the same mechanical performance. Among the categories proposed for the production of these systems, considering that functional performance can be high in all cases, it can be concluded claiming the greater versatility allowed by melt-MEX systems in terms of composition, however, there is a prevalence of ink-MEX systems for specific types of remediation, with more sensitive fillers.

It should be pointed out that the main current limitation for these technologies lies in the difficulty of achieving high porosity. Although the manufacturing processes for these 3D systems are simpler and faster than traditional processes for producing 2D or 1D systems, the latter provide higher porosity and greater surface area, thus higher removal efficiency. However, 3D systems are mechanically more stable, so they can be used for more cycles.

Then, future perspectives should include the implementation of advanced combinated processes, such as melt-mex processes involving selective leaching, aimed at increasing porosity and surface area of 3D systems while preserving their mechanical robustness. Architectures could also be more developed, aiming at increasing surface area through complex schemes, as already beginning to be explored; in addition, it would be interesting to evaluate how the geometry of the system affects the contact times between absorber and pollutant, through fluid dynamic analysis and multidisciplinary approaches.

Additional implementations should be conducted on fillers, which, in all categories, emerge as useful in enhancing the functionality of 3D systems; while the incorporation of these fillers into the systems should be optimized, it is essential to find alternative fillers to traditional ones with lower costs and easy processing. Recently, also in this context, attention is turning toward natural fillers produced from waste masses, which, in addition to promoting the transition to a circular economy, often exhibit adsorptive properties toward various pollutants.

In conclusion, the continuous evolution and improvement of 3D systems for the removal of aqueous pollutants represent a promising path toward more sustainable and effective solutions to address water pollution. For optimal results, it is essential to know and carefully select the most advantageous combinations of materials and production technologies. These choices must be based on the specific properties needed to treat different types of pollutants, thus ensuring targeted and sustainable effectiveness.

CRediT authorship contribution statement

Roberto Scaffaro: Writing – review & editing, Writing – original draft, Visualization, Validation, Supervision, Resources, Project administration, Methodology, Investigation, Funding acquisition, Formal analysis, Data curation, Conceptualization. **Maria Chiara Mistretta:** Writing – review & editing, Writing – original draft, Visualization, Validation, Supervision, Project administration, Methodology, Investigation, Formal analysis, Data curation, Conceptualization. **Marta Balsamo:** Writing – review & editing, Writing – original draft, Visualization, Validation, Methodology, Investigation, Formal analysis, Data curation.

Funding sources

This research was funded by SiciliAn MicronanOTecH Research Additionally, Innovation Center —SAMOTHRACE, European Commission ECS00000022, CUP: B73C22000810001.

Declaration of competing interest

The authors declare that they have no known competing financial interests or personal relationships that could have appeared to influence the work reported in this paper.

Abbreviations

MEX	Material Extrusion
3DBP	3D Bioprinintg
DIW	Direct Ink Writing
SLA	Stereolithography
DLP	Digital Light Processing
S_A	Surface Area
P	Porosity
d_P	Pore diameter
WCA	Water Contact Angle
E	Elastic Modulus
CS	Compressive strength
TS	Tensile Strength
MS	Maximum Strength
R_E	Removal Efficiency
t_T	Treatment time

Data availability

No data was used for the research described in the article.

References

[1] A. Prüss-Üstün, C. (Carlos) Corvalán, R. Bos, M. Neira, World Health Organization, Preventing Disease through Healthy Environments : a Global Assessment of the Burden of Disease from Environmental Risks, n.d.

[2] R. Fuller, P.J. Landrigan, K. Balakrishnan, G. Bathan, S. Bose-O'Reilly, M. Brauer, J. Caravanos, T. Chiles, A. Cohen, L. Corra, M. Cropper, G. Ferraro, J. Hanna, D. Hanrahan, H. Hu, D. Hunter, G. Janata, R. Kupka, B. Lanphear, M. Lichtveld, K. Martin, A. Mustapha, E. Sanchez-Triana, K. Sandilya, L. Schaefli, J. Shaw, J. Seddon, W. Suk, M.M. Téllez-Rojo, C. Yan, Pollution and health: a progress update, Lancet Planet. Health 6 (2022) e535–e547, https://doi.org/10.1016/S2542-5196(22)00090-0.

[3] T. Münzel, O. Hahad, A. Daiber, P.J. Landrigan, Soil and water pollution and human health: what should cardiologists worry about? Cardiovasc. Res. 119 (2023) 440–449, https://doi.org/10.1093/cvr/cvac082.

[4] Water for prosperity and peace water for prosperity and peace the united nations World water development Report 2024. www.unesco.org/en/open-access/cc-sa, 2024.

[5] F. Kordbacheh, & Golnaz Heidari, Materials Chemistry Horizons REVIEW Water Pollutants and Approaches for Their Removal, Mater. Chem. Horizons 2023 (n.d.) 139–153. https://doi.org/10.22128/MCH.2023.684.1039.

[6] N. Asghar, A. Hussain, D.A. Nguyen, S. Ali, I. Hussain, A. Junejo, A. Ali, Advancement in nanomaterials for environmental pollutants remediation: a systematic review on bibliometrics analysis, material types, synthesis pathways, and related mechanisms, J. Nanobiotechnol. 22 (2024), https://doi.org/10.1186/s12951-023-02151-3.

[7] W.A. Al-Amrani, S.A. Onaizi, Adsorptive removal of heavy metals from wastewater using emerging nanostructured materials: a state-of-the-art review, Sep. Purif. Technol. (2024) 127018, https://doi.org/10.1016/j.seppur.2024.127018.

[8] A.S. Mramba, P.P. Ndibewu, L.L. Sibali, K. Makgopa, A review on electrochemical degradation and biopolymer adsorption treatments for toxic compounds in pharmaceutical effluents, Electroanalysis 32 (2020) 2615–2634, https://doi.org/10.1002/elan.202060454.

[9] L. Rani, J. Kaushal, A.L. Srivastav, P. Mahajan, A critical review on recent developments in MOF adsorbents for the elimination of toxic heavy metals from aqueous solutions, (n.d.). https://doi.org/10.1007/s11356-020-10738-8/Published.

[10] V.S. Solanki, B. Pare, P. Gupta, S.B. Jonnalagadda, R. Shrivastava, A review on advanced oxidation processes (AOPs) for wastewater remediation, Asian J. Chem. 32 (2020) 2677–2684, https://doi.org/10.14233/ajchem.2020.22806.

[11] S. Alipoori, H. Rouhi, E. Linn, H. Stumpfl, H. Mokarizadeh, M.R. Esfahani, A. Koh, S.T. Weinman, E.K. Wujcik, Polymer-based devices and remediation strategies for emerging contaminants in water, ACS Appl. Polym. Mater. 3 (2021) 549–577, https://doi.org/10.1021/acsapm.0c01171.

[12] A. Subash, M. Naebe, X. Wang, B. Kandasubramanian, Fabrication of biodegradable fibrous systems employing electrospinning technology for effluent treatment, Environmental Science: Advances 2 (2022) 368–396, https://doi.org/10.1039/d2va00244b.

[13] J.M. Rocha, R.P.C.L. Sousa, R. Fangueiro, D.P. Ferreira, The potential of electrospun membranes in the treatment of textile wastewater: a review, Polymers 16 (2024), https://doi.org/10.3390/polym16060801.

[14] B. Balusamy, O.F. Sarioglu, A. Senthamizhan, T. Uyar, Rational design and development of electrospun nanofibrous biohybrid composites, ACS Appl. Bio Mater. (2019), https://doi.org/10.1021/acsabm.9b00308.

[15] T. Sfetsas, S. Patsatzis, A. Chioti, A review of 3D printing techniques for bio-carrier fabrication, J. Clean. Prod. 318 (2021), https://doi.org/10.1016/j.jclepro.2021.128469.

[16] J.D. Kechagias, Surface roughness assessment of ABS and PLA filament 3D printing parts: structural parameters experimentation and semi-empirical modelling, Int. J. Adv. Manuf. Technol. (2024), https://doi.org/10.1007/s00170-024-14232-0.

[17] N.A. Fountas, K. Kitsakis, K.E. Aslani, J.D. Kechagias, N.M. Vaxevanidis, An experimental investigation of surface roughness in 3D-printed PLA items using design of experiments, Proc. IME J. J. Eng. Tribol. 236 (2022) 1979–1984, https://doi.org/10.1177/13506501211059306.

[18] J. Kechagias, S. Zaoutsos, Effects of 3D-printing processing parameters on FFF parts' porosity: outlook and trends, Mater. Manuf. Process. 39 (2024) 804–814, https://doi.org/10.1080/10426914.2024.2304843.

[19] R. Selvakumar, A. Guhananthan, T. Palanisami, Recent advances in micropollutant removal and mitigation from water using three dimensional adsorbent materials, Curr. Opin. Environ. Sci. Health 34 (2023), https://doi.org/10.1016/j.coesh.2023.100475.

[20] D. Saidulu, A. Srivastava, A.K. Gupta, Enhancement of wastewater treatment performance using 3D printed structures: a major focus on material composition, performance, challenges, and sustainable assessment, J. Environ. Manag. 306 (2022), https://doi.org/10.1016/j.jenvman.2022.114461.

[21] A.P. Fagundes, J.O.D.B. Lira, N. Padoin, C. Soares, H.G. Riella, Additive manufacturing of functional devices for environmental applications: a review, J. Environ. Chem. Eng. 10 (2022), https://doi.org/10.1016/j.jece.2022.108049.

[22] P. Ghosal, B. Gupta, R.S. Ambekar, M.M. Rahman, P.M. Ajayan, N. Aich, A. K. Gupta, C.S. Tiwary, 3D printed materials in water treatment applications, Adv. Sustain. Syst. 6 (2022), https://doi.org/10.1002/adsu.202100282.

[23] S. Roy Barman, P. Gavit, S. Chowdhury, K. Chatterjee, A. Nain, 3D-Printed materials for wastewater treatment, JACS Au 3 (2023) 2930–2947, https://doi.org/10.1021/jacsau.3c00409.

[24] S. Siddiqui, S. Surananai, K. Sainath, M. Zubair Khan, R. Raja Pandiyan Kuppusamy, Y. Kempaiah Suneetha, Emerging trends in development and application of 3D printed nanocomposite polymers for sustainable environmental solutions, Eur. Polym. J. 196 (2023), https://doi.org/10.1016/j.eurpolymj.2023.112298.

[25] J.Z.Y. Tan, M.A. Ávila-López, A. Jahanbakhsh, X. Lu, J. Bonilla-Cruz, T.E. Lara-Ceniceros, J.M. Andresen, M.M. Maroto-Valer, 3D direct ink printed materials for chemical conversion and environmental remediation applications: a review, J. Mater. Chem. A. Mater. 11 (2023) 5408–5426, https://doi.org/10.1039/d2ta08922j.

[26] N. Fijoł, A. Aguilar-Sánchez, A.P. Mathew, 3D-printable biopolymer-based materials for water treatment: a review, Chem. Eng. J. 430 (2022), https://doi.org/10.1016/j.cej.2021.132964.

[27] R. Nisticò, A comprehensive study on the applications of clays into advanced technologies, with a particular attention on biomedicine and environmental remediation, INORGA 10 (2022), https://doi.org/10.3390/inorganics10030040.

[28] H. Zhang, Y. Xue, C. Jiang, D. Liu, L. Zhang, G. Lang, T. Mao, D.B. Effrem, T. Iimaa, U. Surenjav, M. Liu, 3-Dimensional printing of polysaccharides for water-treatment: a review, Int. J. Biol. Macromol. 265 (2024), https://doi.org/10.1016/j.ijbiomac.2024.131117.

[29] Y. Xue, M. Kamali, X. Zhang, N. Askari, C. De Preter, L. Appels, R. Dewil, Immobilization of photocatalytic materials for (waste)water treatment using 3D printing technology – advances and challenges, Environ. Pollut. 316 (2023), https://doi.org/10.1016/j.envpol.2022.120549.

[30] T. Sfetsas, S. Patsatzis, A. Chioti, A review of 3D printing techniques for bio-carrier fabrication, J. Clean. Prod. 318 (2021), https://doi.org/10.1016/j.jclepro.2021.128469.

[31] Y. Pinyakit, P. Romphophak, P. Painmanakul, V.P. Hoven, Introduction of an ambient 3D-printable hydrogel ink to fabricate an enzyme-immobilized platform with tunable geometry for heterogeneous biocatalysis, Biomacromolecules 24 (2023) 3138–3148, https://doi.org/10.1021/acs.biomac.3c00202.

[32] A. Rybarczyk, W. Smułek, A. Grzywaczyk, E. Kaczorek, T. Jesionowski, L. D. Nghiem, J. Zdarta, 3D printed polylactide scaffolding for laccase immobilization to improve enzyme stability and estrogen removal from wastewater, Bioresour. Technol. 381 (2023), https://doi.org/10.1016/j.biortech.2023.129144.

[33] R. Scaffaro, F. Lopresti, V. Catania, S. Santisi, S. Cappello, L. Botta, P. Quatrini, Polycaprolactone-based scaffold for oil-selective sorption and improvement of bacteria activity for bioremediation of polluted water: porous PCL system obtained by leaching melt mixed PCL/PEG/NaCl composites: oil uptake performance and bioremediation efficiency, Eur. Polym. J. 91 (2017) 260–273, https://doi.org/10.1016/j.eurpolymj.2017.04.015.

[34] A. Bandyopadhyay, S. Bose, S. Das, 3D printing of biomaterials, MRS Bull. 40 (2015) 108–114, https://doi.org/10.1557/mrs.2015.3.

[35] A. Jandyal, I. Chaturvedi, I. Wazir, A. Raina, M.I. Ul Haq, 3D printing – a review of processes, materials and applications in industry 4.0, Sustain. Operat. Compu. 3 (2022) 33–42, https://doi.org/10.1016/j.susoc.2021.09.004.

[36] A.P. Fagundes, J.O.D.B. Lira, N. Padoin, C. Soares, H.G. Riella, Additive manufacturing of functional devices for environmental applications: a review, J. Environ. Chem. Eng. 10 (2022), https://doi.org/10.1016/j.jece.2022.108049.

[37] S. Siddiqui, S. Surananai, K. Sainath, M. Zubair Khan, R. Raja Pandiyan Kuppusamy, Y. Kempaiah Suneetha, Emerging trends in development and application of 3D printed nanocomposite polymers for sustainable environmental solutions, Eur. Polym. J. 196 (2023), https://doi.org/10.1016/j.eurpolymj.2023.112298.

[38] M. Baechle-Clayton, E. Loos, M. Taheri, H. Taheri, Failures and flaws in fused deposition modeling (FDM) additively manufactured polymers and composites, J. Compos. Sci. 6 (2022), https://doi.org/10.3390/jcs6070202.
[39] A. GhavamiNejad, N. Ashammakhi, X.Y. Wu, A. Khademhosseini, Crosslinking strategies for 3D bioprinting of polymeric hydrogels, Small 16 (2020), https://doi.org/10.1002/smll.202002931.
[40] Y. Liu, X. Xia, Z. Liu, M. Dong, The next frontier of 3D bioprinting: bioactive materials functionalized by bacteria, Small 19 (2023), https://doi.org/10.1002/smll.202205949.
[41] M.A.S.R. Saadi, A. Maguire, N.T. Pottackal, M.S.H. Thakur, M.M. Ikram, A. J. Hart, P.M. Ajayan, M.M. Rahman, Direct ink writing: a 3D printing technology for diverse materials, Adv. Mater. 34 (2022), https://doi.org/10.1002/adma.202108855.
[42] F. Lupone, E. Padovano, F. Casamento, C. Badini, Process phenomena and material properties in selective laser sintering of polymers: a review, Materials 15 (2022), https://doi.org/10.3390/ma15010183.
[43] J. Huang, Q. Qin, J. Wang, A review of stereolithography: processes and systems, Processes 8 (2020), https://doi.org/10.3390/PR8091138.
[44] R. Chaudhary, P. Fabbri, E. Leoni, F. Mazzanti, R. Akbari, C. Antonini, Additive manufacturing by digital light processing: a review, Progr. Addit. Manufact. 8 (2023) 331–351, https://doi.org/10.1007/s40964-022-00336-0.
[45] Z. Jiang, B. Diggle, M.L. Tan, J. Viktorova, C.W. Bennett, L.A. Connal, Extrusion 3D printing of polymeric materials with advanced properties, Adv. Sci. 7 (2020), https://doi.org/10.1002/advs.202001379.
[46] J.W. Stansbury, M.J. Idacavage, 3D printing with polymers: challenges among expanding options and opportunities, in: Dental Materials, Elsevier Inc., 2016, pp. 54–64, https://doi.org/10.1016/j.dental.2015.09.018.
[47] M. Hofmann, 3D printing gets a boost and opportunities with polymer materials, ACS Macro Lett. 3 (2014) 382–386, https://doi.org/10.1021/mz4006556.
[48] V. Shanmugam, M.V. Pavan, K. Babu, B. Karnan, Fused deposition modeling based polymeric materials and their performance: a review, Polym. Compos. 42 (2021) 5656–5677, https://doi.org/10.1002/pc.26275.
[49] J.M. Jafferson, D. Chatterjee, A review on polymeric materials in additive manufacturing, in: Mater Today Proc, Elsevier Ltd, 2021, pp. 1349–1365, https://doi.org/10.1016/j.matpr.2021.02.485.
[50] T. Sheikh, K. Behdinan, Fused deposition modelling of thermoplastic polymer nanocomposites: a critical review, C (Basel) 10 (2024) 29, https://doi.org/10.3390/c10020029.
[51] A.D. Squires, R.A. Lewis, Feasibility and characterization of common and exotic filaments for use in 3D printed terahertz devices, J. Infrared, Millim. Terahertz Waves 39 (2018) 614–635, https://doi.org/10.1007/s10762-018-0498-y.
[52] P. Ortega-Columbrans, A. Ferrandez-Montero, J. Yus, A.J. Sanchez-Herencia, B. Ferrari, Processing of membranes and 3D scaffolds based on n-TiO2 colloidally dispersed on a thermoplastic matrix for photocatalytic pollutant removal, Catal. Today 426 (2024), https://doi.org/10.1016/j.cattod.2023.114371.
[53] A.D. McQueen, M.L. Ballentine, L.R. May, C.H. Laber, A. Das, M.J. Bortner, A. J. Kennedy, Photocatalytic degradation of polycyclic aromatic Hydrocarbons in water by 3D printed TiO2Composites, ACS Environ. Sci. Technol. Water 2 (2022) 137–147, https://doi.org/10.1021/acsestwater.1c00299.
[54] A. Sangiorgi, Z. Gonzalez, A. Ferrandez-Montero, J. Yus, A.J. Sanchez-Herencia, C. Galassi, A. Sanson, B. Ferrari, 3D printing of photocatalytic filters using a biopolymer to immobilize TiO 2 nanoparticles, J. Electrochem. Soc. 166 (2019) H3239–H3248, https://doi.org/10.1149/2.0341905jes.
[55] A.J. Kennedy, A.D. McQueen, M.L. Ballentine, L.R. May, B.M. Fernando, A. Das, K.L. Klaus, C.B. Williams, M.J. Bortner, Degradation of microcystin algal toxin by 3D printable polymer immobilized photocatalytic TiO2, Chem. Eng. J. 455 (2023), https://doi.org/10.1016/j.cej.2022.140866.
[56] K. Li, Y. De Rancourt De Mimérand, X. Jin, J. Yi, J. Guo, Metal oxide (ZnO and TiO2) and Fe-based metal-organic-framework nanoparticles on 3D-printed fractal polymer surfaces for photocatalytic degradation of organic pollutants, ACS Appl. Nano Mater. 3 (2020) 2830–2845, https://doi.org/10.1021/acsanm.0c00096.
[57] Y.D.R. De Mimérand, K. Li, C. Zhou, X. Jin, X. Hu, Y. Chen, J. Guo, Functional supported ZnO/Bi2MoO6Heterojunction photocatalysts with 3D-printed fractal polymer substrates and produced by innovative plasma-based immobilization methods, ACS Appl. Mater. Interfaces 12 (2020) 43138–43151, https://doi.org/10.1021/acsami.0c12286.
[58] K. Kim, M.C. Ratri, G. Choe, M. Nam, D. Cho, K. Shin, Three-dimensional, printed water-filtration system for economical, on-site arsenic removal, PLoS One 15 (2020), https://doi.org/10.1371/journal.pone.0231475.
[59] S. Fernandez-Velayos, G. Vergara, J.M. Olmos, J. Sanchez-Marcos, N. Menendez, P. Herrasti, E. Mazarío, 3D printed monoliths: from powder to an efficient catalyst for antibiotic degradation, Sci. Total Environ. 906 (2024), https://doi.org/10.1016/j.scitotenv.2023.167376.
[60] N. Fijoł, A. Mautner, E.S. Grape, Z. Bacsik, A.K. Inge, A.P. Mathew, MOF@Cell: 3D printed biobased filters anchored with a green metal-organic framework for effluent treatment, J. Mater. Chem. A. Mater. 11 (2023) 12384–12394, https://doi.org/10.1039/d3ta01757e.
[61] G. Zhou, K.P. Wang, H.W. Liu, L. Wang, X.F. Xiao, D.D. Dou, Y.B. Fan, Three-dimensional polylactic acid@graphene oxide/chitosan sponge bionic filter: highly efficient adsorption of crystal violet dye, Int. J. Biol. Macromol. 113 (2018) 792–803, https://doi.org/10.1016/j.ijbiomac.2018.02.017.
[62] S.S. Park, Y. Park, E. Repo, H.S. Shin, Y. Hwang, Three-dimensionally printed scaffold coated with graphene oxide for enhanced heavy metal adsorption: batch and fixed-bed column studies, J. Water Proc. Eng. 57 (2024), https://doi.org/10.1016/j.jwpe.2023.104658.
[63] L.A. Lagalante, A.J. Lagalante, A.F. Lagalante, 3D printed solid-phase extraction sorbents for removal of volatile organic compounds from water, J. Water Proc. Eng. 35 (2020), https://doi.org/10.1016/j.jwpe.2020.101194.
[64] M. Peñas-Garzón, M.J. Sampaio, Y. Manrique, C.G. Silva, J.L. Faria, Enhanced removal of emerging pollutants through visible light-activated carbon nitride materials immobilized over 3D printed structures, J. Environ. Chem. Eng. 11 (2023), https://doi.org/10.1016/j.jece.2023.111343.
[65] P.L. Marconi, A. Trentini, M. Zawoznik, C. Nadra, J.M. Mercadé, J.G. Sánchez Novoa, D. Orozco, M.D. Groppa, Development and testing of a 3D-printable polylactic acid device to optimize a water bioremediation process, Amb. Express 10 (2020), https://doi.org/10.1186/s13568-020-01081-9.
[66] A. Rybarczyk, W. Smułek, A. Grzywaczyk, E. Kaczorek, T. Jesionowski, L. D. Nghiem, J. Zdarta, 3D printed polylactide scaffolding for laccase immobilization to improve enzyme stability and estrogen removal from wastewater, Bioresour. Technol. 381 (2023), https://doi.org/10.1016/j.biortech.2023.129144.
[67] X. Xia, X. Xu, C. Lin, Y. Yang, L. Zeng, Y. Zheng, X. Wu, W. Li, L. Xiao, Q. Qian, Q. Chen, Microalgal-immobilized biocomposite scaffold fabricated by fused deposition modeling 3D printing technology for dyes removal, ES Mater. Manufact. 7 (2020) 40–50, https://doi.org/10.30919/esmm5f706.
[68] A.J. Kennedy, M.L. Ballentine, A. Das, C.S. Griggs, K. Klaus, M.J. Bortner, Additive manufacturing for contaminants: ammonia removal using 3D printed polymer-zeolite composites, ACS ES T Water 1 (2021) 621–629, https://doi.org/10.1021/acsestwater.0c00131.
[69] A.J. Kennedy, M.L. Ballentine, L.R. May, A. Das, A.J. Bednar, C.S. Griggs, M. S. Hull, M.J. Bortner, Simplifying complex contaminant mixtures: selective ammonia adsorption and toxicity reduction using 3D printable polymer–zeolite, Water Air Soil Pollut. 233 (2022), https://doi.org/10.1007/s11270-022-05606-9.
[70] N. Fijoł, H.N. Abdelhamid, B. Pillai, S.A. Hall, N. Thomas, A.P. Mathew, 3D-printed monolithic biofilters based on a polylactic acid (PLA)-hydroxyapatite (HAp) composite for heavy metal removal from an aqueous medium, RSC Adv. 11 (2021) 32408–32418, https://doi.org/10.1039/d1ra05202k.
[71] Y. Zheng, X. Sun, X. Liu, X. Xia, L. Xiao, C. Cao, Q. Qian, Q. Chen, Improving the removal efficiency of methylene blue on 3D-printed camellia seed powder scaffold using porogen, Ind. Crops Prod. 171 (2021), https://doi.org/10.1016/j.indcrop.2021.113930.
[72] N. Fijoł, A. Aguilar-Sánchez, M.X. Ruiz-Caldas, J. Redlinger-Pohn, A. Mautner, A. P. Mathew, 3D printed polylactic acid (PLA) filters reinforced with polysaccharide nanofibers for metal ions capture and microplastics separation from water, Chem. Eng. J. 457 (2023), https://doi.org/10.1016/j.cej.2022.141153.
[73] Z. Viskadourakis, M. Sevastaki, G. Kenanakis, 3D structured nanocomposites by FDM process: a novel approach for large-scale photocatalytic applications, Appl. Phys. Mater. Sci. Process 124 (2018), https://doi.org/10.1007/s00339-018-2014-6.
[74] M.J. Martín de Vidales, A. Nieto-Márquez, D. Morcuende, E. Atanes, F. Blaya, E. Soriano, F. Fernández-Martínez, 3D printed floating photocatalysts for wastewater treatment, Catal. Today 328 (2019) 157–163, https://doi.org/10.1016/j.cattod.2019.01.074.
[75] K. Miklec, I. Grčić, L. Radetić, I.K. Cingesar, D. Vrsaljko, Photocatalytic oxidation of amoxicillin in CPC reactor over 3D printed TiO2-CNT@PETG static mixers, Coatings 13 (2023), https://doi.org/10.3390/coatings13020386.
[76] A.J. Thakuria, P. Suryavanshi, S. Banerjee, 3D printed cartridges for the removal of pharmaceuticals from water, Talanta. Open 9 (2024), https://doi.org/10.1016/j.talo.2024.100299.
[77] S. Waheed, M. Rodas, H. Kaur, N.L. Kilah, B. Paull, F. Maya, In-situ growth of metal-organic frameworks in a reactive 3D printable material, Appl. Mater. Today 22 (2021), https://doi.org/10.1016/j.apmt.2020.100930.
[78] Z. Liu, X. Xia, W. Li, L. Xiao, X. Sun, F. Luo, Q. Chen, Q. Qian, In situ growth of ca2+-based metal–organic framework on casio3/abs/tpu 3d skeleton for methylene blue removal, Materials 13 (2020) 1–14, https://doi.org/10.3390/ma13194403.
[79] Y. Ji, Y. Ma, Y. Ma, J. Asenbauer, S. Passerini, C. Streb, Water decontamination by polyoxometalate-functionalized 3D-printed hierarchical porous devices, Chem. Commun. 54 (2018) 3018–3021, https://doi.org/10.1039/c8cc00821c.
[80] C. Scheid, S.A. Monteiro, W. Mello, M.C. Velho, J. dos Santos, R.C.R. Beck, M. Deon, J. Merib, A novel honeycomb-like 3D-printed device for rotating-disk sorptive extraction of organochlorine and organophosphorus pesticides from environmental water samples, J. Chromatogr. A 1722 (2024), https://doi.org/10.1016/j.chroma.2024.464892.
[81] I.L. Liakos, A. Mondini, E. Del Dottore, C. Filippeschi, F. Pignatelli, B. Mazzolai, 3D printed composites from heat extruded polycaprolactone/sodium alginate filaments and their heavy metal adsorption properties, Mater. Chem. Front. 4 (2020) 2472–2483, https://doi.org/10.1039/d0qm00159g.
[82] R. Scaffaro, E.F. Gulino, M.C. Citarrella, Multifunctional 3D-printed composites based on biopolymeric matrices and tomato plant (Solanum lycopersicum) waste for contextual fertilizer release and Cu(II) ions removal, Adv. Compos. Hybrid Mater. 7 (2024) 95, https://doi.org/10.1007/s42114-024-00908-4.
[83] L. Sandanamsamy, W.S.W. Harun, I. Ishak, F.R.M. Romlay, K. Kadirgama, D. Ramasamy, S.R.A. Idris, F. Tsumori, A comprehensive review on fused deposition modelling of polylactic acid, Progr. Addit. Manufact. 8 (2023) 775–799, https://doi.org/10.1007/s40964-022-00356-w.
[84] N.A. Fountas, S. Zaoutsos, D. Chaidas, J.D. Kechagias, N.M. Vaxevanidis, Statistical modelling and optimization of mechanical properties for PLA and PLA/Wood FDM materials, in: Mater Today Proc, Elsevier Ltd, 2023, pp. 824–830, https://doi.org/10.1016/j.matpr.2023.08.276.

[85] B. Pandey, P. Singh, V. Kumar, Photocatalytic-sorption processes for the removal of pollutants from wastewater using polymer metal oxide nanocomposites and associated environmental risks, Environ. Nanotechnol. Monit. Manag. 16 (2021), https://doi.org/10.1016/j.enmm.2021.100596.
[86] I.J. Ani, U.G. Akpan, M.A. Olutoye, B.H. Hameed, Photocatalytic degradation of pollutants in petroleum refinery wastewater by TiO2- and ZnO-based photocatalysts: recent development, J. Clean. Prod. 205 (2018) 930–954, https://doi.org/10.1016/j.jclepro.2018.08.189.
[87] C. Cazan, A. Enesca, L. Andronic, Synergic effect of tio2 filler on the mechanical properties of polymer nanocomposites, Polymers 13 (2021), https://doi.org/10.3390/polym13122017.
[88] M.J. Mochane, M.T. Motloung, T.C. Mokhena, T.G. Mofokeng, Morphology and photocatalytic activity of zinc oxide reinforced polymer composites: a mini review, Catalysts 12 (2022), https://doi.org/10.3390/catal12111439.
[89] F. Saleem Ahmed Khan, N. Mujawar Mubarak, Y. Hua Tan, R. Rao Karri, M. Khalid, R. Walvekar, E. Chan Abdullah, S. Ali Mazari, S. Nizamuddin, Magnetic nanoparticles incorporation into different substrates for dyes and heavy metals removal-A Review, (n.d.). https://doi.org/10.1007/s11356-020-10482-z/Published.
[90] G. Ramalingam, R. Pachaiappan, P.S. Kumar, S. Dharani, S. Rajendran, D.V.N. Vo, T.K.A. Hoang, Hybrid metal organic frameworks as an Exotic material for the photocatalytic degradation of pollutants present in wastewater: a review, Chemosphere 288 (2022), https://doi.org/10.1016/j.chemosphere.2021.132448.
[91] Z.U. Zango, K. Jumbri, N.S. Sambudi, A. Ramli, N.H.H.A. Bakar, B. Saad, M.N. H. Rozaini, H.A. Isiyaka, A.H. Jagaba, O. Aldaghri, A. Sulieman, A critical review on metal-organic frameworks and their composites as advanced materials for adsorption and photocatalytic degradation of emerging organic pollutants from wastewater, Polymers 12 (2020) 1–42, https://doi.org/10.3390/polym12112648.
[92] S.Z. Al Sheheri, Z.M. Al-Amshany, Q.A. Al Sulami, N.Y. Tashkandi, M.A. Hussein, R.M. El-Shishtawy, The preparation of carbon nanofillers and their role on the performance of variable polymer nanocomposites, Des. Monomers Polym. 22 (2019) 8–53, https://doi.org/10.1080/15685551.2019.1565664.
[93] L.S. Mokoena, J.P. Mofokeng, A review on graphene (GN) and graphene oxide (GO) based biodegradable polymer composites and their usage as selective adsorbents for heavy metals in water, Materials 16 (2023), https://doi.org/10.3390/ma16062527.
[94] J. Tan, Z. Li, J. Li, J. Wu, X. Yao, T. Zhang, Graphitic carbon nitride-based materials in activating persulfate for aqueous organic pollutants degradation: a review on materials design and mechanisms, Chemosphere 262 (2021), https://doi.org/10.1016/j.chemosphere.2020.127675.
[95] S. Bala, D. Garg, B.V. Thirumalesh, M. Sharma, K. Sridhar, B.S. Inbaraj, M. Tripathi, Recent strategies for bioremediation of emerging pollutants: a review for a green and sustainable environment, Toxics 10 (2022), https://doi.org/10.3390/toxics10080484.
[96] D. Berillo, A. Al-Jwaid, J. Caplin, Polymeric materials used for immobilisation of bacteria for the bioremediation of contaminants in water. https://doi.org/10.3390/polym, 2021.
[97] A. Kausar, Inorganic nanomaterials in polymeric water decontamination membranes, Internat. J. Plastics Technol. 23 (2019), https://doi.org/10.1007/s12588-019-09230-x.
[98] G. Hu, J. Yang, X. Duan, R. Farnood, C. Yang, J. Yang, W. Liu, Q. Liu, Recent developments and challenges in zeolite-based composite photocatalysts for environmental applications, Chem. Eng. J. 417 (2021), https://doi.org/10.1016/j.cej.2021.129209.
[99] S. Pai, & M.S. Kini, R. Selvaraj, ENVIRONMENTAL AND ENERGY MANAGEMENT A review on adsorptive removal of dyes from wastewater by hydroxyapatite nanocomposites, (n.d.). https://doi.org/10.1007/s11356-019-07319-9/Published.
[100] P.R. Yaashikaa, P. Senthil Kumar, S. Karishma, Review on biopolymers and composites – evolving material as adsorbents in removal of environmental pollutants, Environ. Res. 212 (2022), https://doi.org/10.1016/j.envres.2022.113114.
[101] E.H. Backes, S.V. Harb, C.A.G. Beatrice, K.M.B. Shimomura, F.R. Passador, L. C. Costa, L.A. Pessan, Polycaprolactone usage in additive manufacturing strategies for tissue engineering applications: a review, J. Biomed. Mater. Res. B Appl. Biomater. 110 (2022) 1479–1503, https://doi.org/10.1002/jbm.b.34997.
[102] L. Pan, Z. Wang, Q. Yang, R. Huang, Efficient removal of lead, copper and cadmium ions from water by a porous calcium alginate/graphene oxide composite aerogel, Nanomaterials 8 (2018), https://doi.org/10.3390/nano8110957.
[103] R. Scaffaro, M.C. Citarrella, A. Catania, L. Settanni, Green composites based on biodegradable polymers and anchovy (Engraulis Encrasicolus) waste suitable for 3D printing applications, Compos. Sci. Technol. 230 (2022), https://doi.org/10.1016/j.compscitech.2022.109768.
[104] R. Scaffaro, M.C. Citarrella, E.F. Gulino, M. Morreale, Hedysarum coronarium-based green composites prepared by compression molding and fused deposition modeling, Materials 15 (2022), https://doi.org/10.3390/ma15020465.
[105] N.P.F. Gonçalves, S.M. Olhero, J.A. Labrincha, R.M. Novais, 3D-printed red mud/metakaolin-based geopolymers as water pollutant sorbents of methylene blue, J. Clean. Prod. 383 (2023), https://doi.org/10.1016/j.jclepro.2022.135315.
[106] N.P.F. Gonçalves, E.F. da Silva, L.A.C. Tarelho, J.A. Labrincha, R.M. Novais, Simultaneous removal of multiple metal(loid)s and neutralization of acid mine drainage using 3D-printed bauxite-containing geopolymers, J. Hazard Mater. 462 (2024), https://doi.org/10.1016/j.jhazmat.2023.132718.
[107] X. Liu, S. Ma, H. Yang, P. He, X. Duan, D. Jia, P. Colombo, Y. Zhou, 3D-printed green and low-cost porous g-C3N4/geopolymer components for the removal of methylene blue from wastewater, J. Am. Ceram. Soc. 107 (2024) 3068–3082, https://doi.org/10.1111/jace.19654.
[108] G. Franchin, J. Pesonen, T. Luukkonen, C. Bai, P. Scanferla, R. Botti, S. Carturan, M. Innocentini, P. Colombo, Removal of ammonium from wastewater with geopolymer sorbents fabricated via additive manufacturing, Mater. Des. 195 (2020), https://doi.org/10.1016/j.matdes.2020.109006.
[109] S.W. Yoon, S.Y. Kim, J.S. Jeon, S. Oh, S.Y. Chung, J.S. Kim, S.K. Maeng, 3D-printed Chlorella vulgaris biocarriers: a novel approach to wastewater treatment, J. Water Proc. Eng. 57 (2024), https://doi.org/10.1016/j.jwpe.2023.104711.
[110] J. Condi Mainardi, K. Rezwan, M. Maas, Genipin-crosslinked chitosan/alginate/alumina nanocomposite gels for 3D bioprinting, Bioproc. Biosyst. Eng. 45 (2022) 171–185, https://doi.org/10.1007/s00449-021-02650-3.
[111] Y. Li, Z. Di, X. Yan, H. Wen, W. Cheng, J. Zhang, Z. Yu, Biocatalytic living materials built by compartmentalized microorganisms in annealable granular hydrogels, Chem. Eng. J. 445 (2022), https://doi.org/10.1016/j.cej.2022.136822.
[112] Y. Li, S. Peng, K. Li, D. Qin, Z. Weng, J. Li, L. Zheng, L. Wu, C.P. Yu, Material extrusion-based 3D printing for the fabrication of bacteria into functional biomaterials: the case study of ammonia removal application, Addit. Manuf. 60 (2022), https://doi.org/10.1016/j.addma.2022.103268.
[113] J. Liu, X. Shen, Z. Zheng, M. Li, X. Zhu, H. Cao, C. Cui, Immobilization of laccase by 3D bioprinting and its application in the biodegradation of phenolic compounds, Int. J. Biol. Macromol. 164 (2020) 518–525, https://doi.org/10.1016/j.ijbiomac.2020.07.144.
[114] Z. Sun, H. Wen, Z. Di, Y. Zhang, S. Zhang, Z. Zhang, J. Zhang, Z. Yu, Photosynthetic living fiber fabrication from algal-bacterial consortia with controlled spatial distribution, ACS Biomater. Sci. Eng. 9 (2023) 6481–6489, https://doi.org/10.1021/acsbiomaterials.3c00884.
[115] Y. Pinyakit, P. Romphophak, P. Painmanakul, V.P. Hoven, Introduction of an ambient 3D-printable hydrogel ink to fabricate an enzyme-immobilized platform with tunable geometry for heterogeneous biocatalysis, Biomacromolecules 24 (2023) 3138–3148, https://doi.org/10.1021/acs.biomac.3c00202.
[116] M. Schaffner, P.A. Rühs, F. Coulter, S. Kilcher, A.R. Studart, 3D printing of bacteria into functional complex materials. https://www.science.org, 2017.
[117] T. Butelmann, H. Priks, Z. Parent, T.G. Johnston, T. Tamm, A. Nelson, P. J. Lahtvee, R. Kumar, Metabolism control in 3D-printed living materials improves fermentation, ACS Appl. Bio Mater. 4 (2021) 7195–7203, https://doi.org/10.1021/acsabm.1c00754.
[118] A.S. Finny, N. Cheng, O. Popoola, S. Andreescu, 3D printable polyethyleneimine based hydrogel adsorbents for heavy metal ions removal, Environmental Science: Advances 1 (2022) 443–455, https://doi.org/10.1039/d2va00064d.
[119] P. Asghartabar Kashi, A. Mohammadi, J. Chen, R. Ettelaie, H. Jäger, M. Shahbazi, 3D printing of a photo-curable hydrogel to engineer mechanically robust porous structure for ion capture or sustained potassium ferrate(VI) release for water treatment, Sep. Purif. Technol. 344 (2024), https://doi.org/10.1016/j.seppur.2024.127247.
[120] G.A. Appuhamillage, D.R. Berry, C.E. Benjamin, M.A. Luzuriaga, J.C. Reagan, J. J. Gassensmith, R.A. Smaldone, A biopolymer-based 3D printable hydrogel for toxic metal adsorption from water, Polym. Int. 68 (2019) 964–971, https://doi.org/10.1002/pi.5787.
[121] B. Xu, X. Hu, S. Lu, T. Wang, Z. Chen, C. Bai, T. Ma, Y. Song, 3D printing of cellulose nanocrystal-based Pickering foams for removing microplastics, Sep. Purif. Technol. 339 (2024), https://doi.org/10.1016/j.seppur.2024.126642.
[122] M. Shahbazi, H. Jäger, S.J. Ahmadi, M. Lacroix, Electron beam crosslinking of alginate/nanoclay ink to improve functional properties of 3D printed hydrogel for removing heavy metal ions, Carbohydr. Polym. 240 (2020), https://doi.org/10.1016/j.carbpol.2020.116211.
[123] H.N. Abdelhamid, S. Sultan, A.P. Mathew, Three-dimensional printing of cellulose/covalent organic frameworks (celloCOfs) for CO2 adsorption and water treatment, ACS Appl. Mater. Interfaces 15 (2023) 59795–59805, https://doi.org/10.1021/acsami.3c13966.
[124] R. Pei, L. Fan, F. Zhao, J. Xiao, Y. Yang, A. Lai, S.F. Zhou, G. Zhan, 3D-Printed metal-organic frameworks within biocompatible polymers as excellent adsorbents for organic dyes removal, J. Hazard Mater. 384 (2020), https://doi.org/10.1016/j.jhazmat.2019.121418.
[125] H. Nasser Abdelhamid, S. Sultan, A.P. Mathew, Binder-free Three-dimensional (3D) printing of Cellulose-ZIF8 (CelloZIF-8) for water treatment and carbon dioxide (CO2) adsorption, Chem. Eng. J. 468 (2023), https://doi.org/10.1016/j.cej.2023.143567.
[126] Y. Zhang, Y. Chen, Y. Jiang, G. Sui, Self-thickening and self-strengthening 3D printing magnetic cellulose-based aerogel for adsorption and recovery of methylene blue, Adv. Sustain. Syst. 6 (2022), https://doi.org/10.1002/adsu.202100329.
[127] A. Masud, C. Zhou, N. Aich, Emerging investigator series: 3D printed graphene-biopolymer aerogels for water contaminant removal: a proof of concept, Environ. Sci.: Nano 8 (2021) 399–414, https://doi.org/10.1039/d0en00953a.
[128] J.J. Moyano, J. Loizillon, D. Pérez-Coll, M. Belmonte, P. Miranzo, D. Grosso, M. I. Osendi, Robust and conductive mesoporous reduced graphene oxide-silica hybrids achieved by printing and the sol gel route, J. Eur. Ceram. Soc. 41 (2021) 2908–2917, https://doi.org/10.1016/j.jeurceramsoc.2020.09.070.
[129] L. Bergamonti, C. Bergonzi, C. Graiff, P.P. Lottici, R. Bettini, L. Elviri, 3D printed chitosan scaffolds: a new TiO2 support for the photocatalytic degradation of amoxicillin in water, Water Res. 163 (2019), https://doi.org/10.1016/j.watres.2019.07.008.

[130] C. Li, Y. Zhang, C. Qiu, B. Yuan, R. Zhang, W. Li, H. Jin, Powder-precursor integrated 3D-printed TiO2 photocatalyst and adsorption-degradation synergy effect, Colloids Surf. A Physicochem. Eng. Asp. 671 (2023), https://doi.org/10.1016/j.colsurfa.2023.131570.
[131] H.H. Do, T.K.C. Tran, T.D.T. Ung, N.T. Dao, D.D. Nguyen, T.H. Trinh, T.D. Hoang, T.L. Le, T.T.H. Tran, Controllable fabrication of photocatalytic TiO2 brookite thin film by 3D-printing approach for dyes decomposition, J. Water Proc. Eng. 43 (2021), https://doi.org/10.1016/j.jwpe.2021.102319.
[132] P. Sun, L. Zhang, S. Tao, Preparation of hybrid chitosan membranes by selective laser sintering for adsorption and catalysis, Mater. Des. 173 (2019), https://doi.org/10.1016/j.matdes.2019.107780.
[133] R. Li, S. Yuan, W. Zhang, H. Zheng, W. Zhu, B. Li, M. Zhou, A. Wing-Keung Law, K. Zhou, 3D printing of mixed matrix films based on metal-organic frameworks and thermoplastic polyamide 12 by selective laser sintering for water applications, ACS Appl. Mater. Interfaces 11 (2019) 40564–40574, https://doi.org/10.1021/acsami.9b11840.
[134] M. Grandcolas, A. Lind, 3D-printed polyamide structures coated with TiO2 nanoparticles, towards a 360-degree rotating photocatalytic reactor, Mater. Lett. 307 (2022), https://doi.org/10.1016/j.matlet.2021.131044.
[135] D. Zhang, J. Xiao, Q. Guo, J. Yang, 3D-printed highly porous and reusable chitosan monoliths for Cu(II) removal, J. Mater. Sci. 54 (2019) 6728–6741, https://doi.org/10.1007/s10853-019-03332-y.
[136] D. Wang, T. Zhi, L. Liu, L. Yan, W. Yan, Y. Tang, B. He, L. Hu, C. Jing, G. Jiang, 3D printing of TiO2 nano particles containing macrostructures for As(III) removal in water, Sci. Total Environ. 815 (2022), https://doi.org/10.1016/j.scitotenv.2021.152754.
[137] A. Bansiddhi, G. Panomsuwan, C. Hussakan, T.L. Htet, B. Kandasamy, K. Janbooranapinij, N. Choophun, R. Techapiesancharoenkij, H.R. Pant, W. L. Ang, O. Jongprateep, Ecofriendly 3D printed TiO2/SiO2/polymer scaffolds for dye removal, Top. Catal. 66 (2023) 1662–1673, https://doi.org/10.1007/s11244-023-01864-x.
[138] P. Blyweert, J. Restivo, O.S.G.P. Soares, V. Nicolas, V. Fierro, M.F.R. Pereira, A. Celzard, First insight into the catalytic activity of stereolithographically 3D-printed tannin-based carbon architectures, ChemCatChem (2024), https://doi.org/10.1002/cctc.202400190.
[139] B. Kandasamy, A. Al Mahmud, J. Lee, I. Hasan, G. Palanisamy, Advancing the eradication of harmful dyes through stereolithography-produced 3D floating photocatalysis: exploiting the synergistic potential of graphene/MnO2/Fe3O4 hybrid nanomaterials, Surface. Interfac. 48 (2024), https://doi.org/10.1016/j.surfin.2024.104302.
[140] G. Proano-Pena, A.L. Carrano, D.M. Blersch, Analysis of very-high surface area 3D-printed media in a moving bed biofilm reactor for wastewater treatment, PLoS One 15 (2020), https://doi.org/10.1371/journal.pone.0238386.
[141] X. Xu, T. Pose-Boirazian, G. Eibes, L.E. McCoubrey, J. Martínez-Costas, S. Gaisford, A. Goyanes, A.W. Basit, A customizable 3D printed device for enzymatic removal of drugs in water, Water Res. 208 (2022), https://doi.org/10.1016/j.watres.2021.117861.
[142] A. Figuerola, D.A.V. Medina, A.J. Santos-Neto, C.P. Cabello, V. Cerdà, G. T. Palomino, F. Maya, Metal–organic framework mixed-matrix coatings on 3D printed devices, Appl. Mater. Today 16 (2019) 21–27, https://doi.org/10.1016/j.apmt.2019.04.011.
[143] L. Burratti, F. Bertelà, M. Sisani, I. Di Guida, C. Battocchio, G. Iucci, P. Prosposito, I. Venditti, Three-dimensional printed filters based on poly(ethylene glycol) diacrylate hydrogels doped with silver nanoparticles for removing Hg(II) ions from water, Polymers 16 (2024), https://doi.org/10.3390/polym16081034.
[144] D.H. Kim, S.H. Nam, G. Han, S.R. Park, G.H. Jeong, S. Kim, Y.T. Cho, N.X. Fang, Robust catalyst 3D microarchitectures by digital light printing with ceramic particle-polymer composites, Apl. Mater. 12 (2024), https://doi.org/10.1063/5.0189594.
[145] V.T. Huong, B. Van Duc, N.T. An, T.T.P. Anh, T.M. Aminabhavi, Y. Vasseghian, S. W. Joo, 3D-Printed WO3-UiO-66@reduced graphene oxide nanocomposites for photocatalytic degradation of sulfamethoxazole, Chem. Eng. J. 483 (2024), https://doi.org/10.1016/j.cej.2024.149277.
[146] R. Singh, G. Souillard, L. Chassat, Y. Gao, X. Mulet, C.M. Doherty, Fabricating bioactive 3D metal–organic framework devices, Adv. Sustain. Syst. 4 (2020), https://doi.org/10.1002/adsu.202000059.
[147] H.S. Far, M. Najafi, M. Hasanzadeh, M. Rabbani, Self-supported 3D-printed lattices containing MXene/metal-organic framework (MXOF) composite as an efficient adsorbent for wastewater treatment, ACS Appl. Mater. Interfaces 14 (2022) 44488–44497, https://doi.org/10.1021/acsami.2c13830.
[148] W. Han, L. Kong, M. Xu, Advances in selective laser sintering of polymers, Int. J. Extrem. Manuf. 4 (2022), https://doi.org/10.1088/2631-7990/ac9096.
[149] M. Pagac, J. Hajnys, Q.P. Ma, L. Jancar, J. Jansa, P. Stefek, J. Mesicek, A review of vat photopolymerization technology: materials, applications, challenges, and future trends of 3d printing, Polymers 13 (2021) 1–20, https://doi.org/10.3390/polym13040598.